Received: 30 November 2021 | Revised: 19 January 2022 | Accepted: 29 January 2022

DOI: 10.1002/agt2.185

Aggregate Open Access WILEY

REVIEW

# Down-conversion materials for organic solar cells: Progress, challenges, and perspectives

**Ram Datt**[1] | **Swati Bishnoi**[2] | **Harrison Ka Hin Lee**[1] | **Sandeep Arya**[3] | **Sonal Gupta**[4] | **Vinay Gupta**[5] | **Wing Chung Tsoi**[1]

[1] Faculty of Science and Engineering, Sustainable Product Engineering Centre for Innovative Functional Industrial Coatings, Swansea University, Bay Campus, Fabian Way, Swansea SA1 8EN, UK

[2] Advanced Materials and Metrology Division, Council of Scientific And Industrial Research - National Physical Laboratory, Dr. K. S. Krishnan Marg, New Delhi 110012, India

[3] Department of Physics, University of Jammu, Jammu, Jammu and Kashmir 180006, India

[4] Department of Conducting Polymers, Institute of Macromolecular Chemistry, Czech Academy of Sciences, Prague 6 162 06, Czech Republic

[5] Department of Physics, Khalifa University of Science and Technology, P. O. Box 127788, Abu Dhabi, United Arab Emirates

**Correspondence**
Ram Datt and Wing Chung Tsoi, Faculty of Science and Engineering, Sustainable Product Engineering Centre for Innovative Functional Industrial Coatings, Swansea University, Bay Campus, Fabian Way, Swansea, SA1 8EN, UK.
Email: ram.datt@swansea.ac.uk and w.c.tsoi@swansea.ac.uk

**Funding information**
SPECIFIC Innovation and Knowledge Centre, Grant/Award Number: EP/N020863/1; Council of Scientific & Industrial Research, Grant/Award Number: 31/1(0494)/2018-EMR-1

**Abstract**

Organic solar cells (OSCs) in terms of power conversion efficiency (PCE) and operational lifetime have made remarkable progress during the last decade by improving the active layer materials and introducing new interlayers. The newly developed wide bandgap organic donor and low bandgap acceptor molecules covered the absorption from the visible to the near-infrared region. Whereas the incident high energy region (UV) is not in favor of OSCs. Its absorption causes thermalization losses and photoinduced degradation, which hinders the PCE and lifetime of OSCs. Recently, lanthanide and non-lanthanide-based down-conversion (DC) materials have been introduced, which can effectively convert the high-energy photons (UV) to low-energy photons (visible) and resolve the spectral mismatch losses that limit the absorption of OSCs in high energy incident spectrum. Furthermore, the DC materials also protect the OSCs from UV-induced degradation. The DC materials were also proposed to cross the Shockley-Queisser efficiency limit of the solar cell. In this review, the need for DC materials and their processing method for OSCs have been thoroughly discussed. However, the main emphasis has been given to developing lanthanides and non-lanthanides-based DC materials for OSCs, their applications, and their impact on photovoltaic device performance, stability, and future perspectives.

**KEYWORDS**
down-conversion, down-shifting, lanthanides, organic solar cells, photostability

## 1 | INTRODUCTION

As human civilization gets established, the requirement of energy becomes the soul of their livelihood. Energy is powering human life by running household equipment, communication, transportation, industries, economic growth, and so forth. Global energy utilization and greenhouse gases emission are rising, and it is estimated that both will double in 2050 as compared to 2001.[1] Today, energy sources are facing depletion as we are dependent on fossil fuels whose stocks are limited, and hence society needs to think about alternatives. Sunlight is a green and abundant source of energy that can be easily converted into electricity by using solar cells, and it is also an example of a renewable energy source. Organic solar cells (OSCs) have emerged as cost-effective, non-toxic, solution-processable, and flexible photovoltaic technology, and it has also received tremendous attention from the research community and corporate as it is predicted as an economical and futuristic renewable energy source. [2–4] Recently, their power conversion efficiency (PCE) crossed the barrier of 18%.[5–7] However, a few issues still need to be addressed to establish OSCs as an efficient and a reliable solar cell technology, for example, its low PCE and lifetime. Improving the utilization of the incident solar spectrum can be one of the approaches to advance the performance of the OSCs system. The OSCs have shown an issue with their stability under ambient environments.[8–10] Moisture and oxygen are the main environmental degradation

factors, and researchers have been trying to fix them by using a proper encapsulation process.[11–14] Besides this, light-induced degradation is still a challenge for OSCs, and it can break the long-term stability and efficiency of the devices.[15,16] The photodegradation in OSCs, particularly UV- induced, may affect a multitude of layers rather than just a photoactive layer and could harm the charge transport layer, and results in poor stability of OSCs.[17–21] Sapkota et al. revealed that the electrical conductivity of the hole transport layer (HTL), poly(3,4-ethylenedioxythiophene) polystyrene sulfonate (PEDOT: PSS) was drastically reduced under continuously exposed UV-radiation, whereas the photoactive layer showed a little degradation.[22] The poor OSCs stability under UV-light ascribed to the oxidative degradation of photoactive layer constitute materials, and the fullerene phase affect the performance and device stability after UV light exposure.[23,24] The researchers are replacing the fullerene derivatives acceptors with non-fullerene acceptors (NFAs), and it helped to deliver high-performance OSCs.[25–30] Unfortunately, the NFAs show the burn-in effect and pose a major challenge. Among prominent deterioration factors, UV-induced degradation played a significant role to reduce the device's lifetime.[31,32] Jeong et al. suggested an approach by employing the UV-cut filter (UCF) in the front side of OSCs that blocks the incident light below 403 nm wavelength, and the resultant devices exhibited slow photoinduced degradation as compared to without (w/o) UCF.[33] The devices with filter and w/o filter retain ~90% and ~20% of the initial value after 14 hrs of continuous illumination under reduced intensity (air mass [AM] 1.5G, 80 mW/cm$^2$). The application of UVF could protect the devices from harmful UV radiations. Nevertheless, it is a costly choice, and the utilization of maximum incident spectrum and the low PCE of OSCs has still a big challenge. The researchers are also showing concern about the maximum theoretical limit of solar cells, and it is termed as a detailed balance limit or Shockley-Queisser (SQ) limit. [34] The fundamental losses occur in solar cells due to the non-absorption of low-energy photons and the thermalization phenomenon by high-energy photons absorptions. In general, this is referred as a spectral mismatch between solar cells absorption profile and incident solar spectrum. The concept of ternary blend OSCs has been presented to cover the broad absorption range by optimizing photon harvesting.[35–40] It includes the two donors-one acceptor or two acceptors-one donor molecules in a single photoactive layer.[41,42] Unfortunately, the incident spectrum high energy region is still unutilized. The singlet-exciton-fission (SF) mechanism has been also suggested to improve the PCE of OSCs.[43,44] It is a technique applied to generate the multiexciton in organic molecules.[45] Congreve et al. demonstrated that the SF process could cross the external quantum efficiency over the unity of OSCs.[46] There are a few materials have been reported for SF application in the literature called polydiacetylene,[47] carotenoids,[48] pentacene,[49] tetracene,[50] anthracene,[51] and 10,21-bis(tri-isopropylsilylethynyl) tetrabenzo[a,c,l,n] pentacene,[52] and so forth, and it is very challenging to find the right material. The spectral converter materials were introduced in the solar cells to assist the higher to lower photons energy conversion. This mechanism might help to resolve the spectral mismatch as well as UV-induced degradation in OSCs. By using spectral converters, the efficiency of the existing solar cells can be enhanced, and it may exceed the SQ limit of solar cell efficiency for non-concentrated sunlight under the same assumption of radiative recombination.[53] The down-conversion (DC) mechanism was proposed to modify the incident solar spectram for solar cell at the material level.[54] Lanthanides are the prevalent materials as DC in dye-sensitized solar cell (DSSC), silicon, gallium arsenide (GaAs), and perovskite solar cells for spectral conversion. Recently, non-lanthanides materials such as composite nanophosphors, quantum dots (QDs), carbon and graphene QDs, and organic molecules have also been explored for this purpose. The DC materials are known for enhancing the efficiency and stability of the solar cell. The PCE enhancement in OSCs has largely been achieved by material engineering and its deposition parameters optimization, introducing new buffer layers, and device structure development. There are enormous review articles available in literature related to organic molecules-based solar cells, the evolution of device structure, interfacial layers and structural modification, stabilities, and so forth.[55–58] In this review; we have explained the overview of the DC mechanism in detail, followed by lanthanide and non-lanthanide as DC materials and their spectral conversion mechanism. Furthermore, we will cover their applications in OSCs for stability and efficiency enhancement. This article contains in-deep guidelines and reported experimental details of the DC materials for OSCs. The review article will benefit the researchers working in the domain of luminescent materials and solar cells by providing them with an overview of how the spectral converters can be used to improve the solar cell device performance and stability along with their future perspective.

## 2 | DC AND DOWN-SHIFTING MATERIALS

The DC and down-shifting (DS) materials both convert a high-energy photon to a lower energy photon(s). The DC differs from the DS in terms of their external quantum efficiency (QE); DS shows less than unity, whereas DC has unity or more than unity.[59–61] The DC and DS can absorb high-energy photons (300–500 nm) and convert them into lower-energy photons, and both are useful for solar cells application. In the DC mechanism, the one singlet exciton is converted into two triplet excitons.[62,63] Figure 1A,B illustrates both DS and DC working mechanisms, which shows QE less than 1 and larger than 1 or equal to 1 (100%), respectively. The researchers did not follow that definition in practice and used the DC term for DS property materials.[64] In this review, for simplicity, the DC term has been used for all the reviewed materials. The types of DC materials explored for energy conversion purposes have been categorized into two parts: lanthanide and non-lanthanides. The DC mechanism was first investigated on single lanthanide ions such as $Tm^{3+}$ and $Gd^{3+}$, and later in two ions combination system such as $Gd^{3+}$- $Eu^{3+}$, $Pr^{3+}$-$Yb^{3+}$, and $Tb^{3+}$-$Yb^{3+}$, and so forth., where the one material (donor) transfers the excitation energy to another material (acceptor).[65,66] Wegh et al. have reported the idea of developing DC materials that could deliver external quantum efficiency up to 200% by using lanthanide materials and could be useful for future development of DC material for solar cell application.[67] In non-lanthanides, there are a variety of materials available, for instance, QDs, oxides, organic dyes, luminescent glasses, and

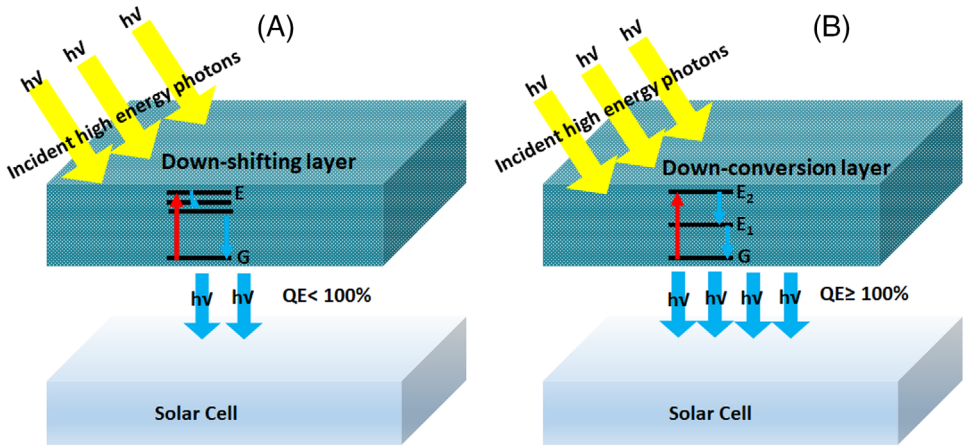


**FIGURE 1** Schematic of (A) down-shifting (DS) and (B) down-conversion (DC) layer attached with solar cells and their energy transfer mechanism

so forth. have been studied. The DC materials were initially applied in luminescent devices such as a fluorescent tube or plasma discharge panels, and so forth., and later were also explored for solar cell application to absorb the unutilized high energy photons.[53,68,69] The theory behind energy transfer rates and model for donor-acceptor interactions was predicted by Förster and Dexter a long time ago.[70,71] The reported DC materials for OSCs have been summarized in Section 4 and are divided into lanthanide and non-lanthanide sections.

## 2.1 | Properties requirement as a DC material

The DC material has been placed on the solar cell or doped into charge transport or photoactive layers. A fraction of the incident photons is absorbed by it, and thereafter, the high-energy photons are down-converted. The selection criteria for ideal DC materials for solar cells application should possess the following characteristics[72]: (i) high photoluminescence quantum efficiency (PLQE), (ii) photochemical and environmental stability, (iii) broadband absorption in the region where the spectral response of the solar cell is low, (iv) high absorption coefficient in low wavelength region, (v) high transmittance and broadband emission, particularly in the region where the device response is high, (vi) sufficient stokes shift to minimize the self-absorption energy losses due to the spectral overlap between the absorption and emission bands, (vii) low cost, (viii) easy to process and can be deposited by the large scalable method, (ix) low film roughness, and (x) easy doping in electron/hole transport or active layer.

## 2.2 | Photophysical test for DC materials

A few characterization techniques are available, which could help to measure the basic properties of the DC materials and it required before implementing them with the OSCs. These are called photophysical properties such as absorption and photoluminescence. In absorption, it is expected that the DC materials should have a high absorption coefficient in the high-energy photons region. It could be helpful to calculate the absorption coefficient of DC materials. Another important property is photoluminescence, which is also needed prior to implementing DC materials. It is suggested to measure DC materials' PLQE, and the high PLQE is good for improving the OSCs performance. It is likely to have unity or more than unity PLQE of DC materials; the more is good.

## 2.3 | DC materials for solar cells

The DC applications in photovoltaic were started a decade back; nevertheless, there is a long history behind the development of the energy transfer phenomenon between two materials. In late 1923, Cario and Franck demonstrated the experimental phenomenon of resonance energy transfer between two materials.[73] They took the mixture of mercury and thallium vapor and irradiated them with light that could only be absorbed by mercury. And the resultant emission spectra belong to the wavelength region that could be emitted by thallium, and it clearly explained the transfer of excitation energy between mercury and thallium. The quantum theory of resonance energy transfer was put forward by Kallman, London, and F. Perrin and was later improved by the notable contribution of Förster and Dexter.[70,71] The classical aspects of energy transfer and the theory of radiative and radiationless in the molecular system were demonstrated by Hans Kuhn and Andrews, respectively.[74,75] Wegh et al. introduced the $Eu^{3+}$ doped $LiGdF_4$ down conversion material for fluorescent lamps and plasma display panels application. The high energy to low energy photon conversion was observed after exposure of $Gd^{3+}$ under UV, and two visible photons were emitted by $Eu^{3+}$.[67] In fluorescent lamps, the phosphors get stuck inside the glass tube wall and convert UV (254 nm) radiation into blue, green, and red light, which ultimately yields white light. The UV excitation with visible emission is also possible with $Gd^{3+}$-$Eu^{3+}$ couple and it shows the DC process. The Er material for DC applications was reported by Oskam et al. in the $Er^{3+}$-$Gd^{3+}$-$Tb^{3+}$ system.[76] Figure 2 shows the simplified energy level diagram of the $Er^{3+}$ -$Gd^{3+}$- $Tb^{3+}$ DC process. After excitation of $Er^{3+}$, cross-relaxation takes place between $Er^{3+}$ and $Gd^{3+}$, and $Er^{3+}$ relaxes by emitting green photons to $Gd^{3+}$. The $Gd^{3+}$ excited energy is transferred through the $Gd^{3+}$ sublattices and finally reaches $Tb^{3+}$ and is emitted as the second photon. The DC energy transfer in $Yb_xY_{1-x}PO^4$:$Tb^{3+}$system from $Tb^{3+}$ to two $Yb^{3+}$ was

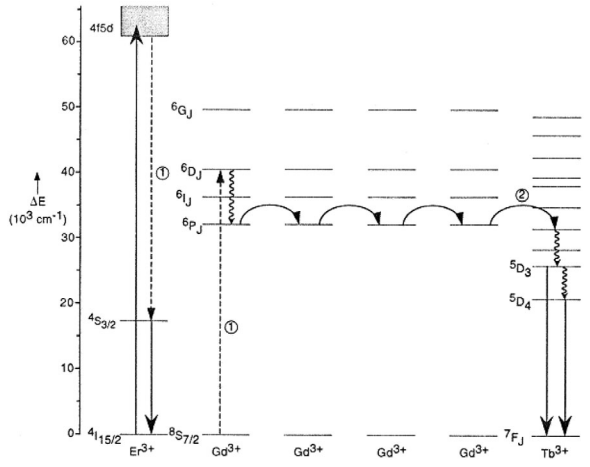


**FIGURE 2** $Er^{3+}$ -$Gd^{3+}$- $Tb^{3+}$system energy level diagram. Reproduced with permission.[76] Copyright © 2000, Elsevier Science S.A. All rights reserved

investigated by Vergeer et al. that was later applied for solar cells application.[77] Yu et al. introduced the $Gd_2O_2S:Tm^{3+}$ as a potential DC material having QE more than 100% for future solar cells application.[78]

## 2.4 | Solar cells efficiency improvement

The spectral distribution of sunlight under AM 1.5 comprises photons with broad wavelengths covering from ultraviolet to infrared (280–2500 nm, 0.5–4.4 eV). Nonetheless, the existing solar cells are able to utilize only a fraction of the incident solar photons, ranging from visible to near-infrared. Figure 3A shows a part of the unutilized high-energy solar spectrum, and it could be employed by using DC materials. Trupke et al. proposed the application of DC materials to manage the high-energy photons and helped to generate more than one electron-hole pair.[53] This phenomenon can be achieved by using DC of high-energy photons. The author calculated the theoretical efficiency limit of the different bandgap solar cells by using a DC system for nonconcentrated sunlight. The PCEs of 38.6% and 39.65%, were reported by applying DC material at the front and rear surface of solar cells, respectively, compared to 30.9% of control device. Figure 3B shows the calculated PCE graph of different bandgap solar cells. Tayebjee et al. demonstrated the theoretical analysis of an overview of the efficiency limit for the range of solar cells devices and proposed that by using a DC system the PCE could reach up to 40.4% and 43.5%, after attaching at front and rear side of the solar cell, respectively. [79] Although, the DC attachment at the front surface is the more practical approach and can be applied with existing solar cells. The advantage of this modification is that the photons having an energy between photoactive layer bandgap (Eg) and 2Eg, which cannot be down-converted, are almost transmitted through the DC layer.

## 2.5 | Solar cell cost reduction

The OSCs is an emerging technology, and the estimation of its exact implementation cost may not be likely at the moment. Kolowekamo et al. derived an OSCs module cost by using a simple model of calculating the module's output and dividing it by the material cost of the same module area.[80] There are other two OSCs module cost analysis methods that have been reported, and in these models, the module performance and stability are the major concern for paying less.[81,82] The DC materials could be beneficial to reduce the OSCs overall cost. The data of reduction in total cost for OSCs after implementing DC materials are not available. In contrast, it is well reported for Si-based solar cells. Donne et al. reported the deposition of polyvinyl acetate (PVA) layer doped with europium (Eu) over commercially available crystalline-silicon (c-Si) solar cell and found that 0.65% enhancement in $J_{sc}$, could decrease the peak wattage ($W_p$) price from 4.55 to 4.49 €/$W_p$. [83] By taking this as a reference, in which the 1.32% price of solar cells could be reduced by using a DC material that can only improve the device performance by 0.65%. However, as explained in Tables 1 and 2, the recently developed DC materials improved the OSCs device performance between 7% and 70%, which was an enormous increment as compared to PVA doped with $Eu^{3+}$ that were investigated for c-Si solar cells. It is suggested that the OSCs cost could be reduced by implementing the DC materials.

# 3 | DC MATERIALS FOR INORGANIC AND DSSC SOLAR CELLS

Initially, the DC mechanism was employed in dye-sensitized solar cells as reported by Kim et al. via using $LiGdF_4$: Eu as spectral converter material.[84] It had excitation at 275 nm and emission around 590 nm and 610 nm wavelength. The emission occurred after excitation energy transfer from gadolinium ($Gd^{3+}$) to europium ($Eu^{3+}$), and the relaxed energy was released in the visible region. A variety of research has also been done on DC materials for the enhancement of solar cells stability. Liu et al., developed a luminescent transparent nanocrystal with a uniform film of lanthanide dysprosium ($Dy^{3+}$) doped $LaVO_4$.[85] The nanocrystals film was coated on the front side of (primary facing the incident solar spectrum), as shown in Figure 4A. The device stability has been studied for DC and control devices under continuous illumination with the Xe lamp light source. Although device stability shows a high impact with $LaVO_4$: Dy coated DC layer, as shown in Figure 4B. An efficiency loss was 50% in the control device, while there were no such losses observed with DC layer coating. The DC layer has protected the dye and electrolyte cells from UV light.

In silicon solar cells, Richards et al. proposed the idea behind the material requirement and implementation of spectral converter layers for Si solar cells.[86,59] Strümpel et al. summarized the DC material requirement for silicon solar cells and mentioned that a material having excitation at a wavelength shorter than 550 nm is a suitable candidate.[87] Hung et al. introduced the colloidal $Ba_2SiO_4$: $Eu^{2+}$ structure and deposited it on the microtextured silicon surface.[88] It improved the $J_{sc}$ from 34 to 34.48 mA/cm$^2$, and the PCE was enhanced from 15.13% to 15.36%. Later, $SiN_x$:$Tb^{3+}$–$Yb^{3+}$, and silicon-rich oxide have also been proposed as DC materials for silicon solar cells.[89,90] Recently, Yao et al. reported the $Tb^{3+}$-$Yb^{3+}$ co-doped $NaYF_4$ nanoparticles (NPs) as DC material for silicon solar cells. [91] Figure 4D shows the J-V

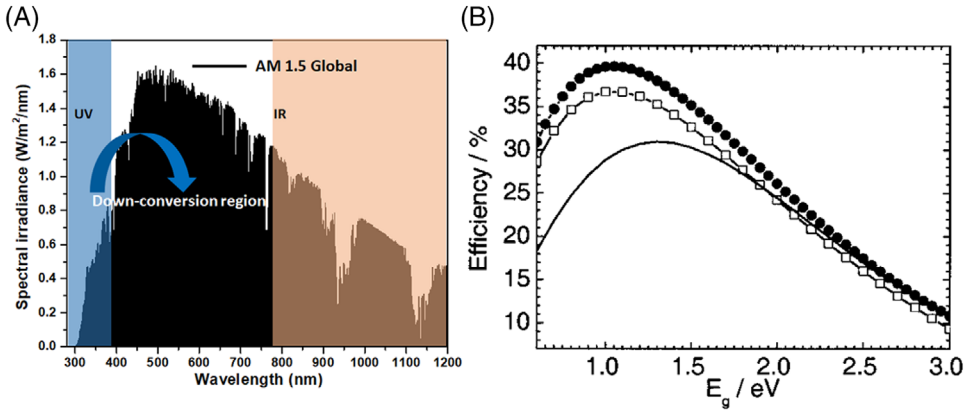


**FIGURE 3** (A) Air mass (AM) 1.5G spectrum, showing the fraction (highlighted in black) absorbed by a Si-based PV cell. The spectral regions marked as blue are available for utilization by down-conversion processes. (B) The efficiency of solar cells system for non-concentrated radiation from a 6000 K Sun: conventional solar cells Shockley-queisser limit (solid line), the efficiency of the solar cells with DC located on the front side (open squares), and the efficiency of the solar cells (solid circles) system with DC on the rear surface. Reproduced with permission.[53] Copyright © 2002, AIP Publishing

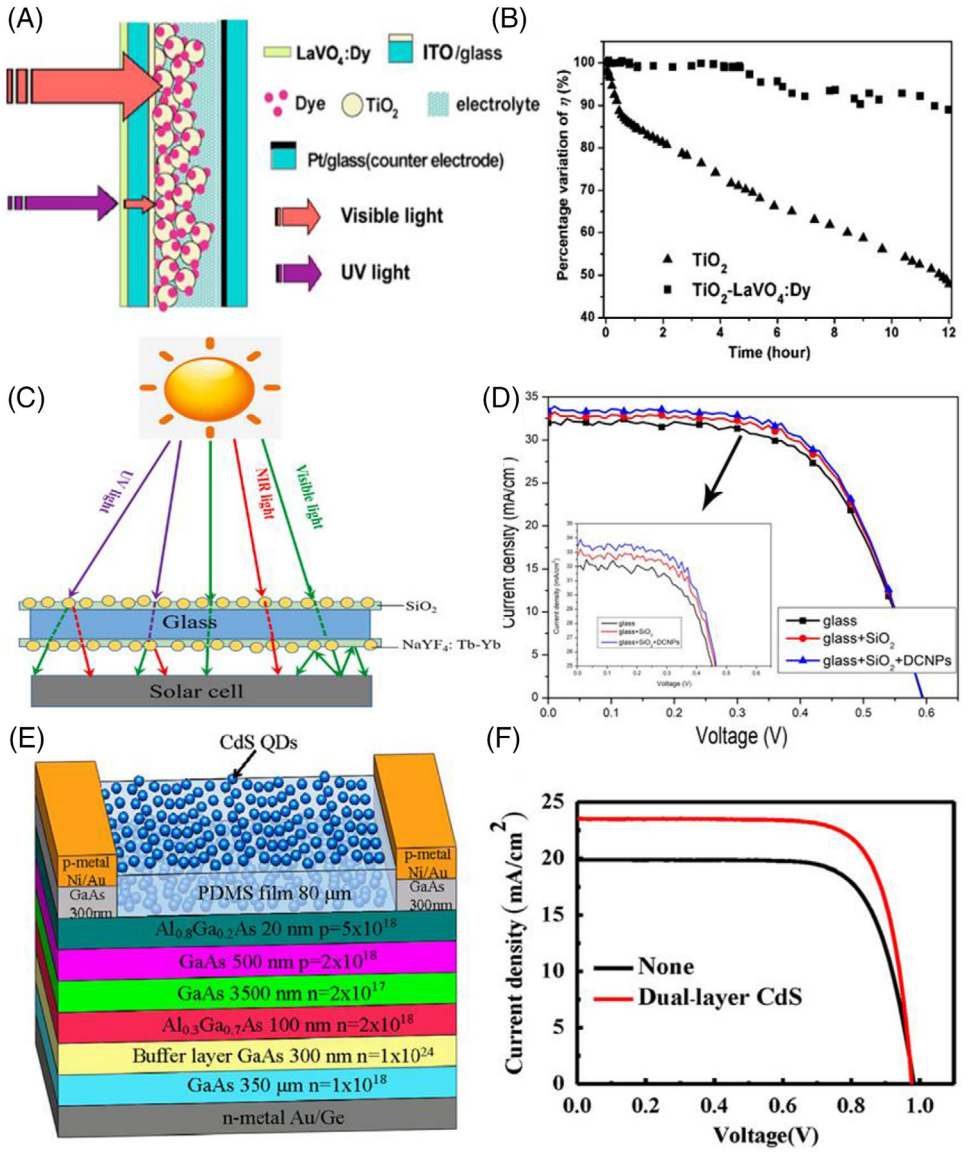


**FIGURE 4** (A) DSSC device structure with lanthanide-based DC nanocrystal layer, (B) DSSC cells stability with and without the DC layer ($LaVO_4$: Dy). Reproduced with permission.[85] Copyright © 2006, AIP Publishing. (C) The measurement illustration of silicon solar cells coated with $SiO_2$, $SiO_2$+ $Tb^{3+}$-$Yb^{3+}$ co-doped $NaYF_4$ ($NaYF_4$: Tb-Yb) and control, and (D) resultant device J-V characteristics (inset zoom graph shows the improvement in current). Reproduced with permission.[91] Copyright © 2020, International Solar Energy Society. Published by Elsevier Ltd. (E) The GaAs solar cell's schematic structure with CdS DC layer, and its (F) J-V characteristics with DC layer and control device. Reproduced with permission.[92] Copyright © 2012, Elsevier B.V

**TABLE 1** A summary of photovoltaic performance of selected lanthanide down-conversion materials-based OSCs devices

| Device structure | DC materials | Active layers (AL) | Absorption/excitation wavelength (nm) | Photoemission peak/band (nm) | $J_{sc}$ (mA/cm$^2$) | $V_{oc}$ (V) | FF(%) | PCE(%) | PCE Increment (%) | References |
|---|---|---|---|---|---|---|---|---|---|---|
| (A) DC/optical filter/ITO/ZnO/AL/$MoO_3$/Ag* | Control | P3HT: PCBM | ~340 | ~580 | $I_{sc\_UV}$ = 13.5 nA | – | – | – | – | [102] |
| | $Sr_2CeO_4$ | | | | $I_{sc\_UV}$ = 77 nA | – | – | – | – | |
| (B) ITO/DC/AL/Ag | Control | P3HT: PCBM | – | – | 6.01 | 0.54 | 36 | 1.16 | 72.17 | [97] |
| | Eu (5%): $TiO_2$ | | | | 9.47 | 0.58 | 44 | 2.47 | | |
| (B) ITO/DC/PEDOT: PSS/ AL /Ca/Al | Control | PBDTTT-C-T: $PC_{71}BM$ | 250- 310 | 490–510 | 15.76 | 0.76 | 59.35 | 7.12 | 0.14 | [98] |
| | NaYbF4: Tb/Eu | | | | 16.06 | 0.75 | 58.22 | 7.13 | | |
| (B) ITO/DC/AL/$MoO_x$/Al | Control | PCDTBT: $PC_{71}BM$ | 300-400 | 450–700 | 11 | 0.87 | 61.7 | 5.9 | 15.62 | [99] |
| | ZnO: Al, Eu | | | | 11.85 | 0.87 | 66.7 | 6.9 | | |
| (B)ITO/DC/AL/Al | Control | PTB7:$PC_{71}BM$ | – | ~619 | 11.7 | 0.61 | 35 | 2.5 | 43.75 | [101] |
| | $Eu^{3+}$: doped PEDOT: PSS | | | | 15.1 | 0.61 | 42 | 3.9 | | |
| (C) ITO/ZnO/DC/AL/$MoO_3$/Ag | Control | PTB7-Th: $PC_{71}BM$ | 330–380 | ~612 | 16.77 | 0.77 | 62.22 | 8.11 | 12.81 | [100] |
| | $Eu(TTA)_3phen_2$ | | | | 17.64 | 0.77 | 68.13 | 9.22 | | |
| | Control | PBDB-T-2F–IT-4F | | | 19.43 | 0.85 | 74.06 | 12.17 | 7.51 | |
| | $Eu(TTA)_3phen_2$ | | | | 20.39 | 0.86 | 74.98 | 13.12 | | |
| (D) ITO/ZnO:DC/Active layer /PEDOT: PSS/Al | Control | P3HT: PCBM | ~244 | ~378 | 4.11 | 0.59 | 47.8 | 1.16 | 15.87 | [103] |
| | $Sr_2CeO_4$ | | | | 4.82 | 0.60 | 46.9 | 1.36 | | |
| (E) ITO/PEDOT:PSS/DC:AL/Al | Control | PTB7: $PC_{71}BM$ | ~340 | ~644 | 14.14 | 0.76 | 66.3 | 7.2 | 20 | [104] |
| | $GdVO_4$:$Sm^{3+}$ | PTB7: $GdVO_4$:$Sm^{3+}$ $PC_{71}BM$ (1:0.1:1.5) | | | 17.13 | 0.76 | 67.1 | 8.8 | | |

*Device measured under mercury UV lamp (254 nm).

**TABLE 2** A summary of photovoltaic performance of non-lanthanide down-conversion materials-based OSCs devices

| Device structure | DC materials | Active layers (AL) | Absorption/excitation wavelength (nm) | Photoemission peak/band (nm) | $J_{sc}$ (mA/cm$^2$) | $V_{oc}$ (V) | FF(%) | PCE(%) | PCE increment (%) | References |
|---|---|---|---|---|---|---|---|---|---|---|
| (A) DC/ITO/PEDOT: PSS/ AL/Al | Control | P3HT: PCBM | ~380 | 450 -650 | 14.16 | 0.61 | 49.3 | 4.3 | – | [117] |
| | m-C1 | | | | 11.39 | 0.61 | 48.3 | 3.4 | | |
| | p-C1 | | | | 11.97 | 0.61 | 48.7 | 3.5 | | |
| (A) DC/ ITO/PEDOT: PSS/AL /Al | Control | P3HT: PCBM | ~395 | ~534 | 4.70 | 0.55 | 28 | 0.73 | – | [121] |
| | CdS QDs | | | | 3.66 | 0.57 | 27 | 0.59 | | |
| (A) DC/ITO/ZnO/AL/PEDOT/Ag | Control | P3HT: PCBM | ~330 | ~500 | 10.59 | 0.56 | 50 | 3.0 | 6.45 | [120] |
| | Ps: NITZ | | | | 11.27 | 0.57 | 51 | 3.2 | | |
| (A) DC/ITO/PEDOT: PSS/AL /LiF/Al | Control | P3HT: $PC_{61}BM$ | ~350 | 520-620 | 10.26 | 0.61 | 54 | 3.38 | 8.49 | [128] |
| | QDs-silica composite | | | | 11.17 | 0.61 | 54 | 3.68 | | |
| (A) DC/ITO/PEDOT: PSS/AL/Al | Control | P3HT: PCBM | ~360 | ~500 | 0.24 | 0.35 | 16 | 1.3 | 37.5 | [127] |
| | KB: C7 | | | | 0.29 | 0.39 | 18 | 1.9 | | |
| (B) ITO/DC/PEIE/AL/$MoO_3$/Ag | Control | p-DTS($FBTTh_2$)$_2$: $PC_{70}BM$ | ~370 | ~545 | 15.4 | 0.77 | 66.5 | 7.9 | 15.20 | [113] |
| | L-ZnO | | | | 17.27 | 0.78 | 68.0 | 9.2 | | |
| (B) ITO/DC/PEDOT: PSS/AL/Ca/Al | Control | P3HT: $PC_{61}BM$ | ~380 | ~540 | 8.21 | 0.63 | 67 | 3.4 | 13.69 | [64] |
| | ES nanofibers | | | | 9.40 | 0.63 | 66 | 3.9 | | |
| | Control | PTB7: PCBM | | | 12.0 | 0.76 | 65 | 6.0 | 4.87 | |
| | ES nanofibers | | | | 12.75 | 0.75 | 66 | 6.3 | | |
| (B) Glass/DC/HC-PEDOT: PSS/AL/LiF/Al | Control | P3HT: $PC_{61}BM$ | ~360 | ~450 | 7.7 | 0.56 | 64 | 2.8 | – | [118] |
| | Silk fibroin | | | | 7.7 | 0.56 | 59 | 2.6 | | |
| (E) ITO/$TiO_2$/DC: AL/$MoO_3$/Ag | Control | PCDTBT: PCBM | ~380 | ~650 | 12.86 | 0.87 | 49.2 | 5.5 | 21.13 | [119] |
| | PFDTBT | | | | 14.32 | 0.87 | 54.7 | 6.8 | | |

characteristics. An improvement in the $J_{sc}$ can be observed after implementing the DC layer. The devices were measured under three different conditions, containing pure glass, glass with $SiO_2$ coating, and glass with $SiO_2$ coating containing DC material, as shown in Figure 4C. For DC layer measurement, the device delivered PCE up to 12.35% and which was 6.74% and 4.58% higher than pure glass, and glass with $SiO_2$ coated condition measurement.

Apart from silicon solar cells, DC materials have also been introduced in GaAs solar cells. Chen et al. demonstrated a 22% PCE improvement in the GaAs solar cells by using CdS QDs as DC material.[92] The CdS QDs were introduced into flexible polydimethylsiloxane films and deposited on top of the GaAs device, as shown in Figure 4E. The main $J_{sc}$ and FF parameters were enhanced from 19.87 to 23.52 mA/cm$^2$ and 74 to 76%, respectively, and the corresponding PCE was changed from 14.36 to 17.45% under 1 sun illumination. Figure 4F shows the device's J-V characteristics. The $J_{sc}$ impact due to an incident spectral modification and deposited DC film also increase the surface conductivity, which decreases the series resistance and results in improving the device FF.[93] In lanthanides, the Eu doped and Yb/Er-doped phosphors has also been studied for GaAs solar cells, and it improved the device PCE from 22.91 to 23.19%.[94]

## 4 | DC MATERIALS FOR OSCs

A variety of DC materials, called lanthanide and non-lanthanide, have been reported for OSCs, and these are covered in the next section. The application of DC materials in the device can be processed in different ways, and it depends on the DC material properties. Figure 5 shows the device geometries for implementing the DC materials. The coating of the DC layer on the front side (Figure 5A) of the devices could be a challenge to maintain, as it includes an extra layer. On the other hand, DC material doped into the bottom charge transport layer (Figure 5D) or in the active layer (Figure 5E) can be the easiest and cost-effective way to implement the DC materials. Tables 1 and 2 summarize the reported DC materials for OSCs so far, and they are arranged according to device structure varying from Figure 5A–E. Scheme 1 shows the molecular structure of organic molecules (donor, acceptor, and DC ) used in this manuscript, and Figure 5F shows the pictorial illustration of DC materials applied in OSCs.

### 4.1 | Lanthanides as DC materials

#### 4.1.1 | Europium

Europium (Eu) is one of the most widely used dopants in DC materials for solar cell application. In 2011, Eu doped LaOF: $Eu^{3+}$ nanocrystals spectral converter was introduced by Gao et al. and demonstrated it for 325–550 nm to 570–710 nm wavelength light conversion.[95] This emission region is in the operating range of most of solar cells. Xu et al. demonstrated the polymer poly(3-hexylthiophene) (P3HT) film photostability enhancement by using the $YVO_4$:$Eu^{3+}$/$Bi^{3+}$ luminescent nano-film.[96] It blocked the UV light and reduced the photo-induced degradation in the film. The luminescent UV blocking layer has a broad UV absorption ranging from 220–400 nm, and its emission peak is around 621 nm. Due to absorption of UV region, the photostability of P3HT polymer has increased by three folds with $YVO_4$:$Eu^{3+}$ /$Bi^{3+}$ nano-film than control film. Örnek et al. incorporated Eu ions into $TiO_2$ nanocrystals ($TiO_2$:Eu) and fabricated the inverted OSCs of P3HT: [6,6]-Phenyl-C61-butyric acid methyl ester (PCBM) blend system at different concentrations of Eu doping into $TiO_2$.[97] The PCE was improved from 1.16% (control) to 2.47% at 5% Eu doping. An improvement was noticed due to an increase in the short circuit current ($J_{sc}$), Fill factor (FF), and open circuit voltage ($V_{oc}$) from 6.01 to 9.47 mA/cm$^2$, 36 to 44%, and 0.54 to 0.58 eV, respectively. The Eu doping not only modified the incident light spectrum but also improved the conductivity of the $TiO_2$ interlayer. Doping of Eu in $TiO_2$ can also increase the Fermi level, electron-hole recombination is reduced at the interface, and an injection of electrons improve from the active layer to the $TiO_2$ interlayer. Jio et al. incorporated Eu-based composite nanocrystal ($NaYbF_4$: Tb/Eu) with phenanthroline (Phen) and thenoyltrifluoroacetone (TTA) organic molecules.[98] The Phen and TTA organic molecules act as UV absorbers and transfer their energy to composite nanocrystals. However, the Eu and Tb played an essential role in energy conversion. The composite ($NaYbF_4$:Tb/Eu@Phen, TTA), which worked as a DC layer, was deposited between ITO and PEDOT: PSS buffer layer. The device fabricated of poly([4,8-bis [5-(2-ethylhexyl)-2-thienyl] benzo[1,2-b:4,5-b′] dithiophene-2,6-diyl] (2-(2-ethyl-1-oxohexyl) thieno [3,4-b]thiophenediyl]) (PBDTTT-C-T): $PC_{71}BM$ blend system has improved its performance by ∼10% of its initial values that revised the PCE from 7.12 to 7.85%. Datt et al. have also reported the Eu-based dual-functional layer that worked as electron transport layer as well as DC layer in OSCs. [99] This dual function layer was prepared from the zinc oxide (ZnO) doped with aluminum (Al) and Eu, named as ZnO: Al, Eu composite, and it was solution-processable and could be coated in a single step. The composite photoemission spectra show overlapping with the active layer absorption region, and that improved the photogenerated current and the main enhancement was observed in the 550 to 650 nm wavelength region, as shown via the EQE curve (Figure 6B). The J-V characteristics (Figure 6C) revealed the effect of the dual-function buffer layer on cell performance, and dual-function layer-based device (Figure 6A) delivered a high $J_{sc}$ and FF, resulting in an improvement of PCE from 5.9 to 6.9%, as compared to control device. The Eu doping concentration in ZnO: Al affects the device performance as shown in Figure 6D, in which the Eu played a promising role in photons energy conversion. Bu et al. introduced the doping of $Eu(TTA)_3$phen (ETP) in ZnO, which enhanced the OSCs efficiency as well as stability.[100] The ZnO has weak fluorescence at 420–675 nm. Whereas the ETP complex is excited by UV photons and emitted red light photons that have well-covered the absorption region of donor polymers, as shown in Figure 6E. For devices, two different donors: poly[4,8-bis(5-(2-ethylhexyl)thiophen-2-yl) benzo[1,2-b;4,5-b'] dithiophene-2,6-diyl-alt- (4-(2-ethylhexyl)-3-fluorothieno [3,4-b]thiophene-)-2-carboxylate-2-6-diyl)] (PTB7-Th) and poly [(2,6-(4,8-bis (5-(2-ethylhexyl-3-fluoro) thiophen-2-yl) -benzo[1,2-b:4,5-b′] dithiophene)) -alt-(5,5-(1′,3′-di-2-thienyl -5′,7′-bis (2-ethylhexyl) benzo [1′,2′-c:4′,5′-c′] dithiophene-4,8-dione)] (PBDB-T-2F) have been studied.

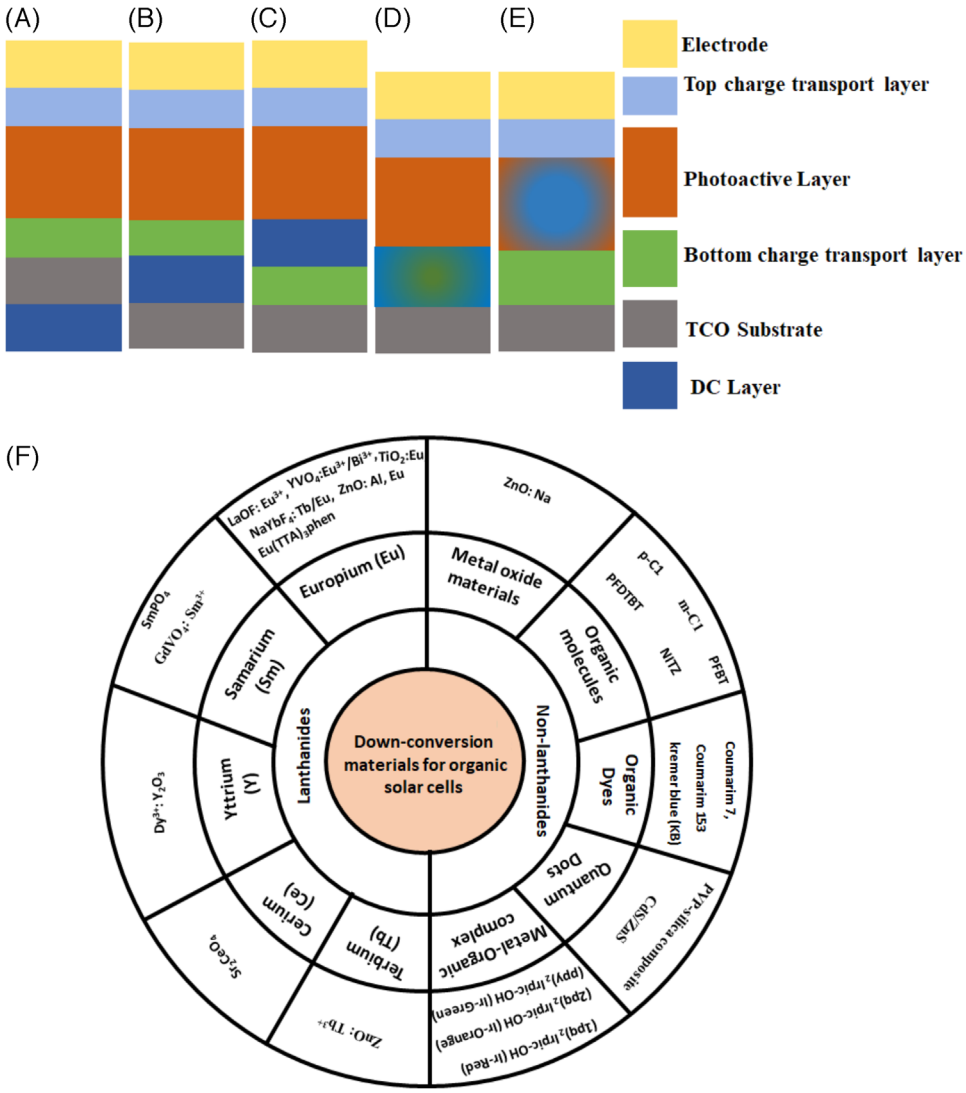


**FIGURE 5** Organic solar cell device geometry with down-conversion (DC) layer coated on (A) the front side of the device, (B) between transparent conductive oxides (TCO) and bottom charge transport layer, (C) between the bottom charge transport layer and photoactive layer, (D) doped in the bottom charge transport layer, (E) doped in the photoactive layer. (F) Schematic illustration of DC materials with their composition reported in OSCs application

The PTB7-Th: $PC_{71}BM$ blend system-based ZnO/ETP complex device has shown a PCE of 9.22% than 8.11% of the control device. Similarly, with PBDB-T-2F-4F: IT-4F blend system, the delivered PCE (13.12%) was higher with ZnO/ETP complex layer than the control device (PCE ~ 12.17%). Moreover, the ZnO/ETP complex-based OSCs have shown better stability than the control device. Figure 6F shows the normalized PCE stability reported for 17 days of device stored under solar light in $N_2$ filled environment. The control device has reached zero efficiencies within ten days, while with ETP complex, the device maintained about 65% of its initial PCE for the same period. The absorption of the UV region by ETP effectively prevents the active layer by UV light and prolongs the lifetime of solar cells. Recently, Mohammad et al. incorporated the Eu ions into PEDOT: PSS HTL, and it was served as a dual function such as charge collection as well as DC layer.[101] The reported device comprising of poly([4,8-bis [(2-ethylhexyl) oxy] benzo[1,2-b:4, 5-b'] dithiophene -2,6-diyl] [3-fluoro-2- [(2-ethylhexyl) carbonyl] thieno [3,4-b] thiophenediyl]) (PTB7): $PC_{71}BM$ blend, and Eu doped HTL showed improvement mainly in $J_{sc}$ and FF, from 11.7 to 15.1 mA/cm$^2$ and 35% to 42%, respectively, and the overall PCE revised from 2.53% to 3.97%.

### 4.1.2 | Samarium

Samarium (Sm) is another popular dopant used in a variety of DC materials. The samarium phosphate ($SmPO_4$) nanophosphors as dopants were introduced by Li et al. into $TiO_2$/P3HT blend inorganic/organic hybrid solar cells (HSCs) and found the PCE of 3% than 1.98% of the control device.[105] In the device, the $TiO_2$ and P3HT worked as acceptors and donors, respectively. The $SmPO_4$ doping effectively regulated the acceptor $TiO_2$ energy levels and improved the charge transport. Figure 7A shows charge carrier movement, optical excitation, and subsequent relaxation mechanism at $SmPO_4/TiO_2$ and P3HT interface. The $SmPO_4$ NPs: $TiO_2$ film has occurred changed in the valence band (VB) and conduction band (CB) from -7.36 to -7.04 eV and -4.33 to -3.76 eV, respectively. The elevation of 0.57 eV and 0.32 eV in CB and VB have occurred and caused an improvement of charge carrier transport as well as in $V_{oc}$. The HSCs were reported at different concentrations (wt%) of $SmPO_3$ nanocrystals, and the optimized results (Figure 7B) were delivered at 5 wt%. Furthermore, major improvements were observed for all three parameters at 0 to 5 wt% $SmPO_4$ doping. The parameters: $V_{oc}$, $J_{sc,}$ and FF showed a gain of 0.67 to 0.71 V, 5.91 to

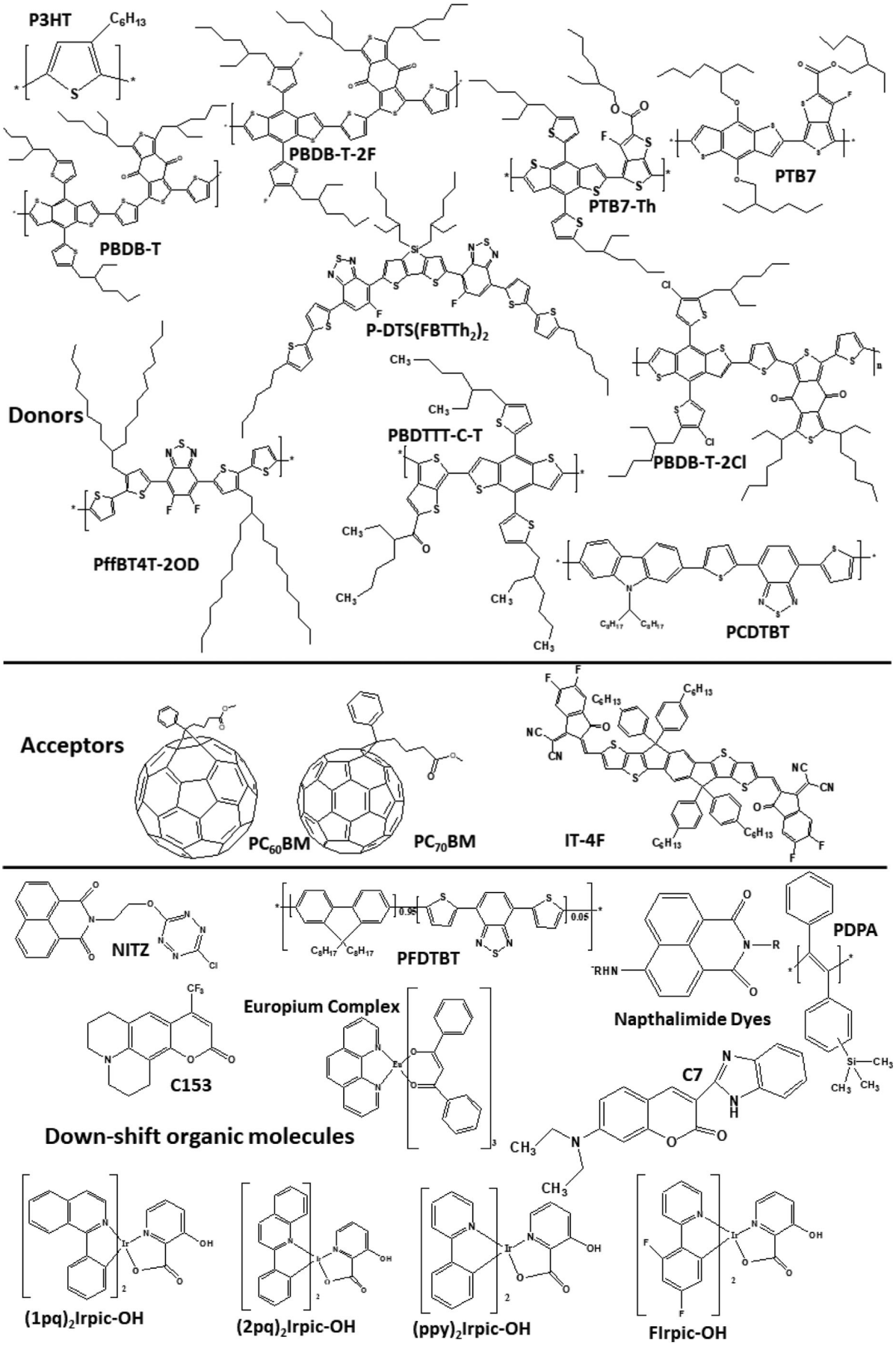


SCHEME 1 Molecular structure of donor, acceptor, and down-conversion (DC) organic molecules

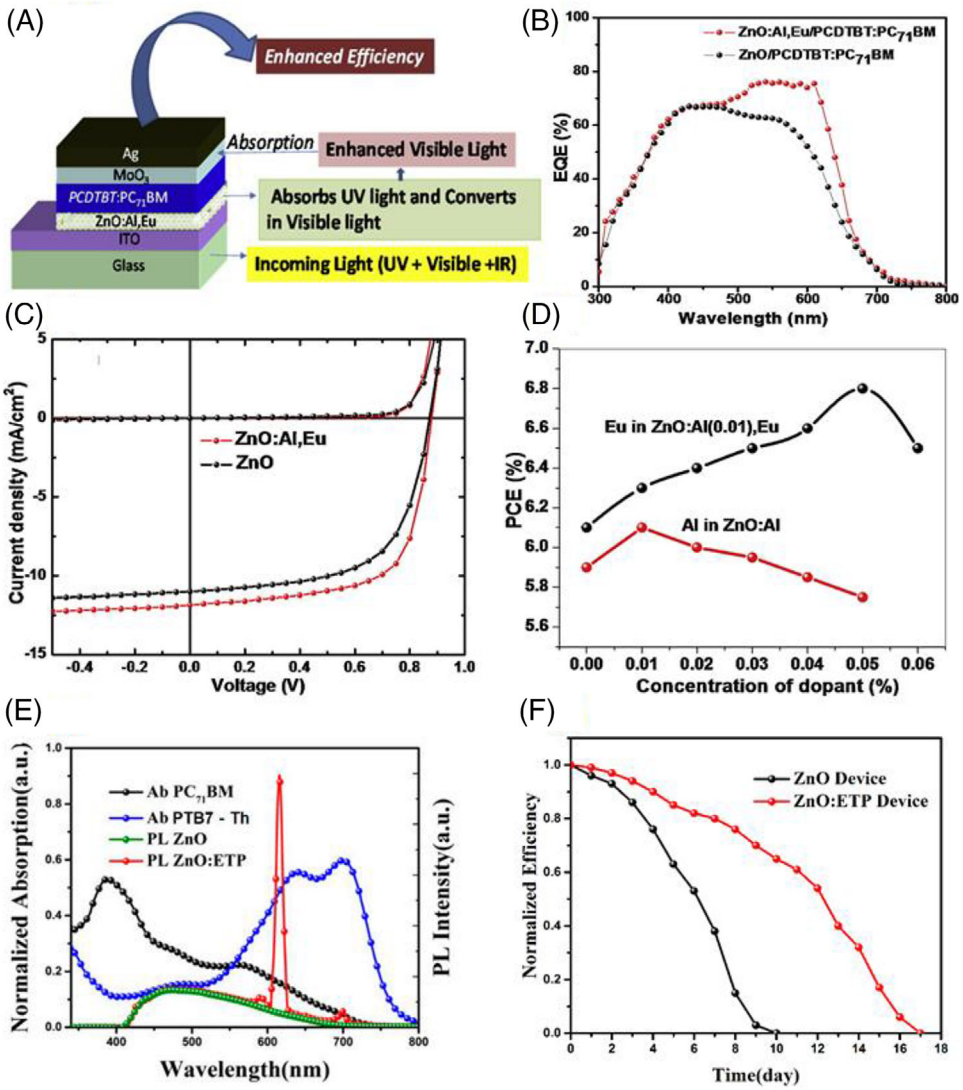


**FIGURE 6** (A) Device geometry of ZnO: Al, Eu as dual function cathode buffer layer with PCDTBT: $PC_{71}BM$ photoactive layer, (B) EQE spectra, and (C) J-V characteristics of optimized ZnO: Al, Eu complex, and pristine ZnO buffer layers-based device. (D) The graph of PCE versus different dopant concentrations (%) of Al and Eu in the ZnO buffer layer. Reproduced with permission.[99] Copyright © 2019, Elsevier B.V. (E) The absorption plot of PTB7-Th, $PC_{71}BM$, and photoluminescence spectra of pristine and $Eu(TTA)_3phen$ (ETP)-doped ZnO film, (F) normalized PCE of ZnO/ETP and control devices, measured over 17 days under the glovebox. Reproduced from CC-BY open access (CC BY 4.0).[100] Copyright © 2020, Bu et al.

7.89 mA/cm$^2$, and 50 to 52%, respectively. Li et al. reported the core-shell nano phosphor of $SmPO_4$ encapsulated into a $Eu^{3+}$ silica shell, as shown in Figure 7C, and the energy transferred from Sm to Eu, which helped in widening the absorption range of $TiO_2$/P3HT HSCs.[106] The core-shell NPs: $TiO_2$/P3HT emission is quenched by 90% compared to pristine P3HT because numerous charge carriers are transported from donor (P3HT) to acceptor (NP: $TiO_2$). As a result, the HSCs devices showed enhancement of PCE from 1.98 to 3.30%. Similarly, Bishnoi et al. introduced Sm-doped luminescent gadolinium orthovanadate ($GdVO_4$: $Sm^{3+}$) QDs into the organic photoactive layer (PTB7: $PC_{71}BM$).[104] The emission region of $GdVO_4$:$Sm^{3+}$ overlaps with absorption spectra of the photoactive layer (Figure 7D), and the $GdVO_4$: $Sm^{3+}$ QDs showed excitation in the near UV region. The doping of QDs into the active layer enhanced the efficiency from 7.2 to 8.8%, as shown in Figure 7E and a significant improvement has occurred in $J_{sc}$ (14.14 to 17.13 mA/cm$^2$) and FF (66 to 67%). The enhancement in the performance of OSCs was attributed to improvement in the active layer morphology after doping with the QDs, and also broadening of the absorption region due to energy transfer between QDs ($GdVO_4$: $Sm^{3+}$) to PTB7: $PC_{71}BM$. The QDs doping prevents the photoactive layer blend (PTB7: $GdVO_4$: $Sm^{3+}$: $PC_{71}BM$) from aggregation and reduces the film roughness. Moreover, the main improvement has been seen in $J_{sc}$ mainly in the photoemission region of the QDs as shown by the EQE graph (Figure 7F).

### 4.1.3 | Yttrium

Yttrium (Y) is used in a variety of luminescent materials; nevertheless, it is more commonly used as a host instead of a dopant. A group in 2014 reported incorporation of hydrothermally synthesized dysprosium ion ($Dy^{3+}$) decorated yttrium oxide ($Dy^{3+}$: $Y_2O_3$) nanocrystals into $TiO_2$, which was used as an acceptor in inorganic/organic HSCs.[107] The $Dy^{3+}$:$Y_2O_3$: $TiO_2$ thin film enhance the light-harvesting and also improve the charge carriers' separation. The $Dy^{3+}$ led to the narrowing of energy level offset between the donor (P3HT) and the acceptor ($Dy^{3+}$: $Y_2O_3$–$TiO_2$), which was

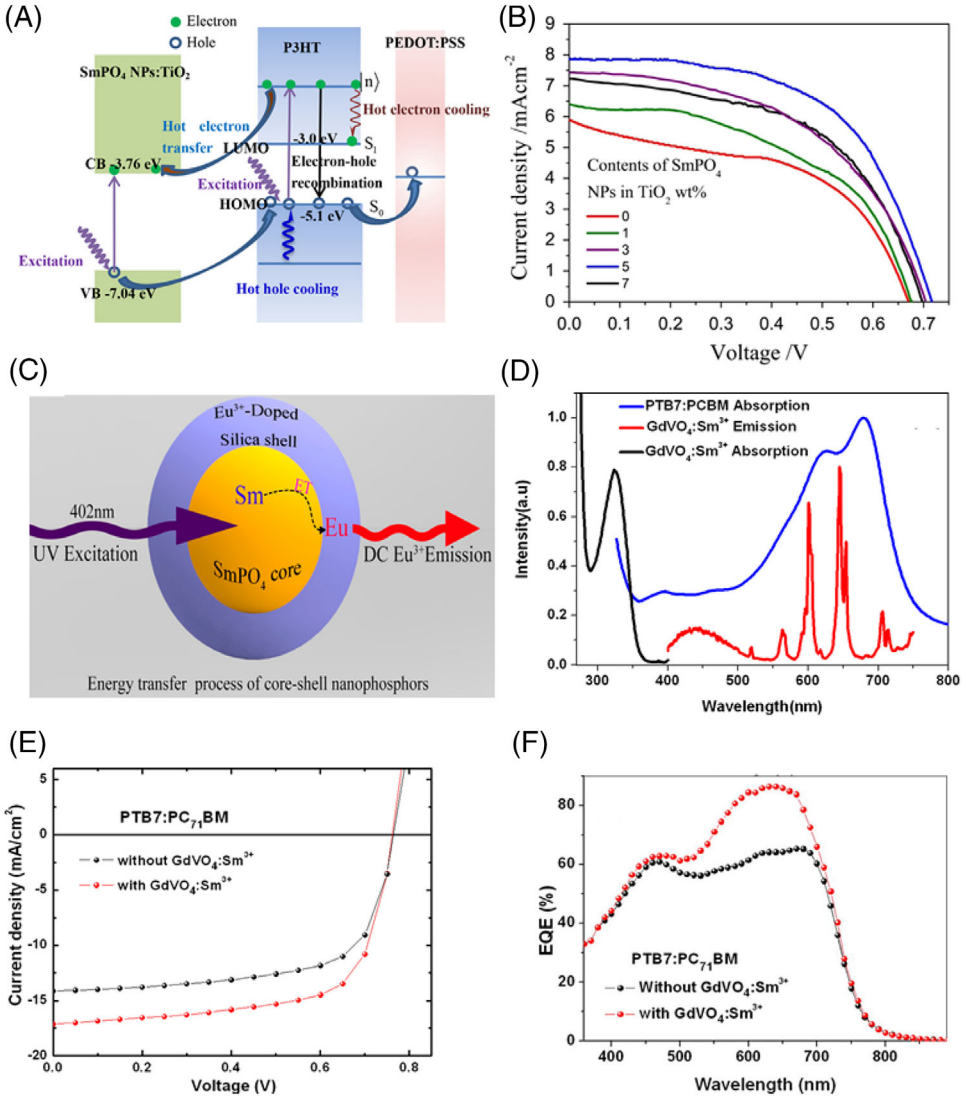


**FIGURE 7** (A) Device structure energy level diagram of $SmPO_4$/P3HT, with an illustration of charge transport, (B) J-V curve of $SmPO_4$: $TiO_2$/P3HT hybrid solar cell. Reproduced with permission.[105] Copyright © 2014, Elsevier B.V. (C) Schematic diagram of core-shell nanoparticles with an energy transfer mechanism. reproduced with permission.[106] Copyright © 2014, American Chemical Society. (D) Combined $GdVO_4$: $Sm^{3+}$ QDs absorption, emission spectra, and PTB7: PCBM photoactive layer absorption spectra, (E) J-V characteristics and (F) EQE curve of OSCs device with and without $GdVO_4$: $Sm^{3+}$ QDs. Reproduced with permission.[104] Copyright © 2016, Swati et al. Rights managed by AIP Publishing

responsible for improving the electron and hole transporting properties. The increase in the amount of $Dy^{3+}$ $Y_2O_3$ in $TiO_2$ from 0 to 6 wt%, increased both $V_{oc}$ and $J_{sc}$ gradually. A maximum PCE of 2.97% was reported under the optimized doping amount of 6.0 wt% of $Dy^{3+}$: $Y_2O_3$ in $TiO_2$, which exhibited higher PCE than the pure $TiO_2$/P3HT HSCs (PCE ~ 2.02%).

### 4.1.4 | Cerium

Dusza et al. introduced the strontium cerium (CE) oxides ($Sr_2CeO_4$) as a DC material in OSCs. [102] The $Sr_2CeO_4$ nanocrystals possess PLQE up to 9.5% at 273 nm excitation. The DC layer was coated on top of the glass slide, and it fitted on the front side of the OSCs during measurement, as shown in Figure 8A. It was measured under UV illumination (254 nm) by applying the UV filter (cut-off the light below 450 nm) or by using a DC layer. The device delivered a very low current of 13.5 nA after applying the UV filter. Whereas, after introducing the luminescent layer coated glass on top of the UV cut-off filter, a slight increase in the current of 77 nA was observed, as shown in Figure 8B. The luminescent nanocrystals utilize high-energy photons for enhancing the OSCs current under UV illumination.

### 4.1.5 | Terbium

Terbium (Tb) is also one of the widely used dopant materials, which was applied in solid-state devices, such as mercury, as well as in low-energy light bulbs.[108] It has an emission region in the visible range, which attracts it as a DC material. Otieno et al. introduced terbium-doped zinc oxide (ZnO: $Tb^{3+}$) for solar cell application.[103] It showed excitation in the UV region and emission in the visible, and it claims its role as a DC layer. The absorption (inset image Figure 8C) of ZnO: $Tb^{3+}$/P3HT: PCBM has increased than the pristine photoactive layer. It shows the constructive role as DC material. The ZnO: $Tb^{3+}$ was coated via RF magnetron sputtering technique and the ITO/ZnO or ZnO: $Tb^{3+}$/P3HT: PCBM/PEDOT: PSS/Al device structure was used. The results (Figure 8C)

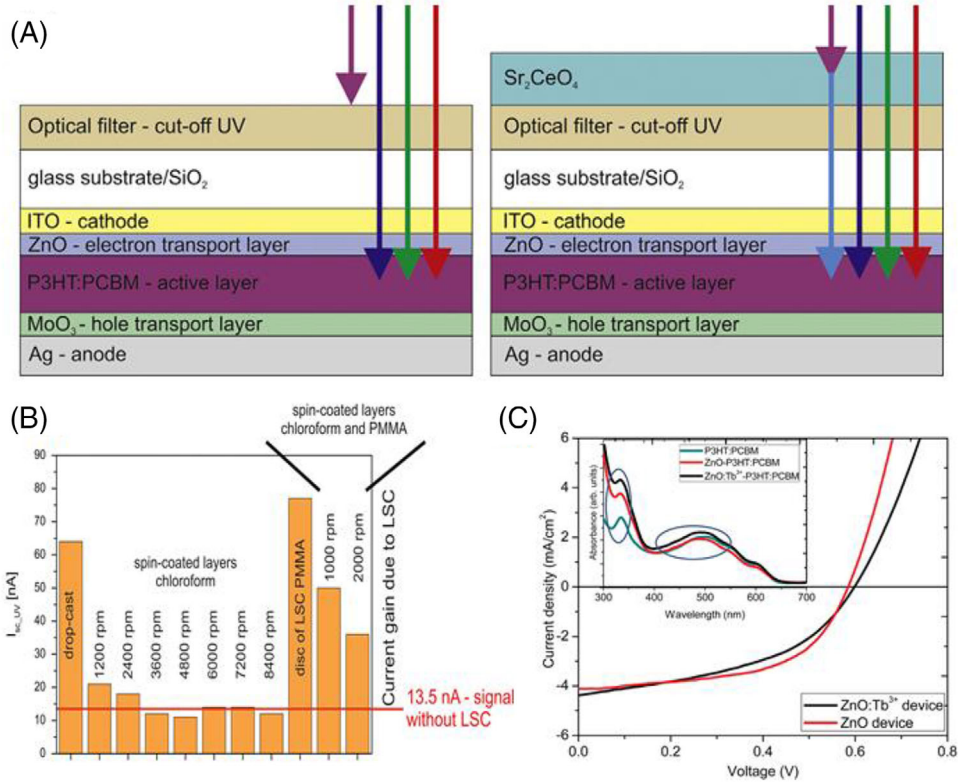


**FIGURE 8** (A) The device structure with and without $Sr_2CeO_4$ coated layer, (B) $J_{sc}$ of the device measured under UV-light. Reproduced with permission.[102] Copyright © 2015, Elsevier B.V. (C) Reported J-V curve of with and without Tb ions doped as cathode layer (inset: the absorption curves of blend layer with different buffer layers) organic solar cells (OSCs) device. Reproduced CC-BY open access (CC-BY: 3.0).[103] Copyright © 2018, Royal society of chemistry

showed the enhancement of PCE from 1.16 to 1.36% after doping Tb into ZnO material.

## 4.2 | Non-lanthanides DC materials

### 4.2.1 | Metal oxide materials

Metal oxide materials have shown attractive optical as well as electrical properties for a wide variety of applications.[109,110] Metal oxides are well reported as charge transport layers in different photovoltaic devices.[111] Sun et al. introduced a thick $TiO_2$ layer in inverted OSCs, and its high thickness served as a UV filter and allowed photoactive layer protection from harmful UV light.[112] Unfortunately, it does not serve as a DC. Nevertheless, a thick $TiO_2$ layer might harm the device performance as it reduces the incident light intensity and loses the photoactive layer absorption. Figure 9A shows the J-V characteristics of fabricated OSCs at a different thickness of $TiO_2$. The thinnest (50 nm) $TiO_2$ device has better performance (PCE ~ 2.41%). However, it lacks device stability under UV light. At thick $TiO_2$ (500 nm), the device PCE (~ 1.19%) gets reduced, and its performance is stable for a long time under UV light, as shown in Figure 9B. It shows the importance of the DC materials to improve both PCE and the stability of the OSCs. In 2016, Bishnoi et al. introduced the sodium doped zinc oxide (ZnO: Na) QDs named luminescent ZnO (L-ZnO) as a DC-based charge transport layer to protect the photoactive layer from UV light and improve the device performance. [113] The L-ZnO absorbs UV light and down converts it into visible light. The emission region of L-ZnO overlap with photoactive layer absorption and led to an enhancement of absorption by the donor molecule. The PCE of L-ZnO-based OSCs has improved from 8% to 9.2% of p-DTS(FBTTh$_2$)$_2$: $PC_{70}BM$ photoactive layer device (Figure 9C). The resultant absorption increased in the case of L-ZnO/p-DTS(FBTTh$_2$)$_2$ than ZnO/ p-DTS(FBTTh$_2$)$_2$, as shown in Figure 9D. Furthermore, photoactive layer absorption mainly improves in the emission region of the L-ZnO (500–650 nm) layer, and it helped to improve the device $J_{sc}$ from 15.4 to 17.27 mA/cm$^2$. In addition to performance improvement, the L-ZnO-based devices have shown better stability under the ambient condition, as shown in Figure 9E. The L-ZnO-based device retains up to 90% of PCE as compared to the pristine ZnO-based device, which was retained only 50% of its initial value within 28 h of the measurement.

### 4.2.2 | Organic molecules/dyes

The organic molecules as a UV filter and DC materials are gaining attention due to their low-cost and easy processability.[114] A few molecules like polyacetylene are very unstable in an ambient environment under heating and intense UV light irradiation. Whereas the side-chain substitution by a bulky group can efficiently improve the photo and thermo-oxidative degradation of polyacetylene.[115] Especially, the protection can be maximized when the electron-resonant aromatic group is substituted. In the aromatic polyacetylenes, the molecules become highly stable under heating or light irradiation. The diphenylacetylene polymer (PDPA)

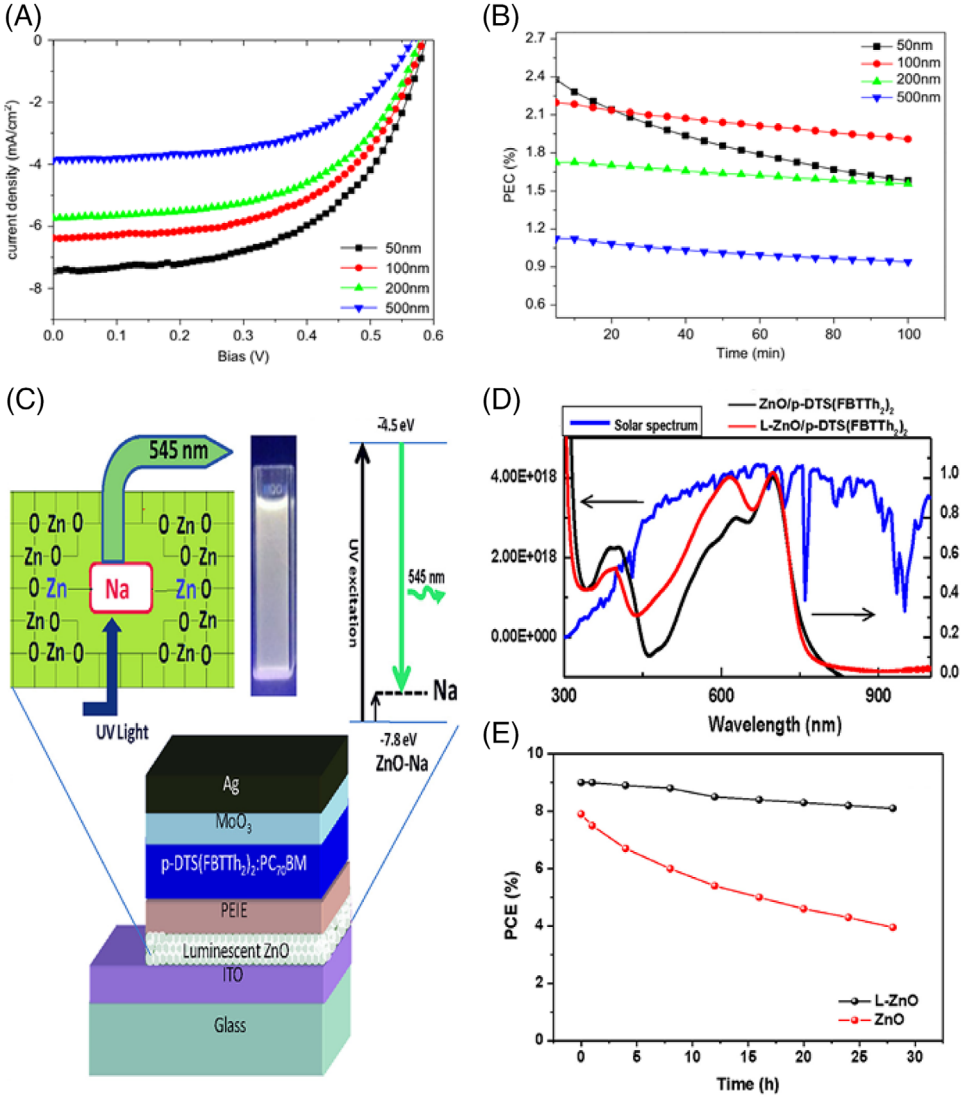


**FIGURE 9** (A) J-V characteristics of different thickness $TiO_2$ buffer layer-based device (ITO/$TiO_2$/P3HT: PCBM/PEDOT: PSS/Ag), (B) stability of different thickness $TiO_2$ based devices under UV illumination. Reproduced with permission.[112] Copyright © 2011, Elsevier B.V. (C) Schematic illustration of device structure and emission mechanism of L-ZnO inserted layer (inset: the solution filled in a cuvette), (D) solar spectrum (photon counts on left Y-axis), and absorption (right Y-axis) of donor molecules after coating on top of pristine and L-ZnO layer, (E) stability of the encapsulated device measured as a function of storage time in ambient condition. Reproduced with permission.[113] Copyright © 2016, Elsevier B.V

derivative is an example of aromatic disubstituted acetylene polymers, and these molecules are glassy and amorphous in nature and also exhibit fluorescence in the visible region.[116] Han et al. introduced the two different PDPA derivatives, namely p-C1 and m-C1, and implemented them to improve the operational lifetime of OSCs.[117] In their study, p-C1 showed strong UV absorption and highly intensive fluorescence emission, which overlap with the donor (P3HT) absorption. A film was coated at the front side of the devices, and it reduced the UV-light-induced degradation. However, the performance of molecules coated devices were observed to be inferior as compared to their control device because the DC film reduced the incident light intensity. The m-C1, p-C1, and the control devices showed PCE of 3.4%, 3.5%, and 4.3%, respectively. Whereas the p-C1 molecule-based device showed high stability under UV radiation. Chen et al. incorporated the dual functional electrospun (ES) nanofibers that contained poly(2,7-[9, 9-dihexylfluorene]-alt- 4,7-[2,1,3-benzothiadiazole]) (PFBT) NPs.[64] The ES nanofibers were directly integrated into two different devices of P3HT and PTB7 donor molecules-based devices in the ITO/DC/PEDOT: PSS/active layer/Ca/Al device structure. A significant improvement was shown in PCE from 3.49% to 4.11% and 6.05% to 7.12% for P3HT and PTB7 donors-based devices, respectively, thereby showing a net enhancement of 18% as compared to control devices. Prosa et al. introduced the water processable DC material. It is prepared from pristine silk fibroin (SF) protein and doped with a derivative of stilbene (STB).[118] The resultant DC material has been applied in ITO-free and P3HT: PCBM photoactive layer-based OSCs (glass/DC/PEDOT: PSS/P3HT: $PC_{61}BM$/LiF/Al). The device with DC did not perform well in terms of performance, and the PCE was 2.6% than the control (PCE ~ 2.8%). Nevertheless, the DC device showed better stability (up to 70 days inside the glove box at room temperature) with a 0% drop in $J_{sc}$ and only 6% reduction in PCE, whereas the control device showed a reduction in PCE by 13%. Liu et al. introduced the PFDTBT polymer QDs, and it worked as DC material.[119] The QDs have been incorporated into the PCDTBT: $PC_{71}BM$ photoactive layer to improve the utilization of the UV light, and the maximum PCE was delivered up to 6.81%, and it was 23.8%

higher than the control device (PCE ~ 5.5%). The QDs doping into the photoactive layer helped in improving the energy band alignment, and as a result, the charge carrier mobility and $V_{oc}$ of the device were improved. Three (0.029, 0.058, 0.087 wt%) different concentrations of QDs were doped into the active blend, and the 0.058 wt% delivered the optimized performance (Figure 10A). Recently, Ourahmoun et al. introduced the yellow-emitting tetrazine molecule called N-(2-[6-chloros- tetrazin-3-yloxy] ethyl)-naphthalimide (NITZ), and it was doped with polystyrene (PS), and reported as DC material for OSCs. [120] The NITZ layer was coated on the separate glass substrate and fixed near the device during measurement. An emission (Figure 10B) spectrum of NITZ solution was reported at different concentrations and showed a high ratio of UV absorbance and photoemission in the visible region. The optimized performance was obtained at a 2% concentration of NITZ, and PCE was 3.28% than 3.08% for the control device. Moreover, the device with the NITZ layer showed a longer lifetime than the control device by possibly reducing the effect of UV degradation.

Organic dyes have gained popularity in imaging, sensors, and solar cells applications due to their fluorescent behavior.[123,124] Recently, it has been investigated as a DC material, and it possesses the following important properties: high absorptivity and PLQY, low cost, and availability in abundance.[125] Fernandes et al. introduced the three different organic dyes and showed their absorption spectra below 450 nm and photoluminescence within the P3HT: PCBM active layer absorption range.[126] These are coumarim 7 (C7), coumarim 153 (C153), and kremer blue (KB). The metal/organic complex ($Alq_3$), and europium complex (Eu) were used to compared the dye's optical properties. To prepare the films, these dyes were mixed in commercially available poly (methyl methacrylate) (PMMA) with chlorobenzene. They showed the PLQY of 37.4%, 20.2%, 9.2%, 30.0%, and 55.5% of C153, C7, KB, Alq3, and Eu, respectively. After mixing the two dyes in different ratios, these have shown remarkable improvement in the PLQY. It is notable that by using the KB: C153 and KB: C7 mixtures, the PLQY values are substantially higher, 88.0 and 38.8%, respectively, than their individual components. Later, Perdomo et al. applied the KB and C7 dyes by mixing at different ratios for solar cells application.[127] The layer was coated on quartz substrates and put on front side of the device (ITO/PEDOT: PSS/P3HT: PCBM/Al) during J-V measurement. An increment of 18.6% was reported in the $J_{sc}$, from 0.24 to 0.29 mA/cm$^2$ with a $Kb_{92.5}C7_{7.5}$ dye, and it contributed to the PCE improvement from 1.37% to 1.99%.

### 4.2.3 | Quantum dots

QDs are 3D confined particles that exhibit excellent photoluminescence properties and high absorption coefficients. The QDs are a superior class of semiconductors that can be crystalline or amorphous and have two- or three-dimensional structures. These are prepared from periodic groups of II-VI, III-V, or IV-VI materials.[129] The adjustable energy gap of QDs allows its application in many fields, including solar cells, and recently, it has emerged as a DC material in OSCs.[130] Aoki et al. applied a layer of cadmium sulfide (CdS) QDs encapsulated in zinc sulfide (CdS/ZnS), and it acts as DC material.[121] The calculated value of PLQY was 38%, which describes how efficiently QDs convert an excitation light into fluorescence. Thus, it shows great potential as a DC material. The DC layer was cast on the front side of the ITO/PEDOT: PSS/P3HT: PCBM/Al device. For the fresh device, the performance with DC and control devices delivered the PCE of 0.59% and 0.73%, respectively. However, it is worth noticing that the DC-based device degradation was lower under continuous light exposure for 120 min as compared to control device. The values of $J_{sc}$, FF, and PCE reduction were higher in control than DC-based devices, as shown in Figure 10C,D. An increase of $J_{sc}$ with QDs DC layer device could be caused by the DC effect and prevent the active layer degradation. Recently, Lim et al. introduced the gradient quantum dot @polyvinylpyrrolidone (PVP)-silica composite as a DC material.[128] The prepared DC material was applied in the ITO/PEDOT: PSS/P3HT: $PC_{61}BM$/LiF/Al device via spin-coating on the front side of the device. Different concentrations of 0.1, 0.3, 0.5 wt% in silica matrix were prepared, and it directly affected the device performance. For 0.1 wt% QDs, the $J_{sc}$ (11.17 mA/cm$^2$) was improved than the control (10.26 mA/cm$^2$) device, and it contributed in improving the PCE from 3.38% to 3.68%. The increasing amount of QDs (0.3 and 0.5 wt%) in the DC layer gradually decreases the PCE and $J_{sc}$ values. These imply that increasing the amount of QDs in the DC layer results in the reduction in the transmittance of the incident light.

### 4.2.4 | Metal-organic complex

Metal-organic complexes, combining approach has shown the ability to tune its optical properties and owing potential application for low-cost printed plastic electronics, as well as optoelectronic devices.[131,132] Recently, metal-organic complex materials also emerged as DC materials and were used as dopants in the donor molecules of the OSCs. Kim et al. introduced the four different iridium-organic complexes, named as $(1pq)_2$ Irpic-OH (Ir-Red), $(2pq)_2$ Irpic-OH (Ir-Orange), $(ppy)_2$ Irpic-OH (Ir-Green), and FIrpic-OH (Ir-blue).[122] The iridium (Ir (III)) complexes have exhibited high quantum yield, control of molecular compatibility, long exciton lifetime, and increased energy transfer efficiency. The iridium complexed molecules served as DC materials, and they were doped into donor molecules (PTB7/P3HT). Figure 10E shows the optical properties of iridium complexes, and the Ir-orange has absorption and photoemission in a region where PTB7/P3HT donor molecules revealed low and high absorption, respectively. For ITO/ZnO/ Ir (III) complexes: PTB7: $PC_{71}BM$ or Ir (III) complexes (Figure 10F): P3HT: $PC_{61}BM$ / $MoO_3$/Ag device structure, the improvement was observed in the $J_{sc}$ and FF of the device of PTB7, from 13.3 to 16.1 mA/cm$^2$, and 71.7% to 72.9%, respectively. The resulting PCE improved from 7.37% to 8.72% for Ir- Orange complex (10 wt%) device. Similarly, for P3HT molecule devices at 0.5 wt% Ir-blue, $J_{sc}$ and FF have increased significantly from 10.3 to 11.5 mA/cm$^2$, and 51.7% to 55.9%, respectively, and the corresponding PCE has improved from 3.02% to 3.63%. The metal-organic complex strategy could improve the PCE and $J_{sc}$ by 18% and 21%, respectively.

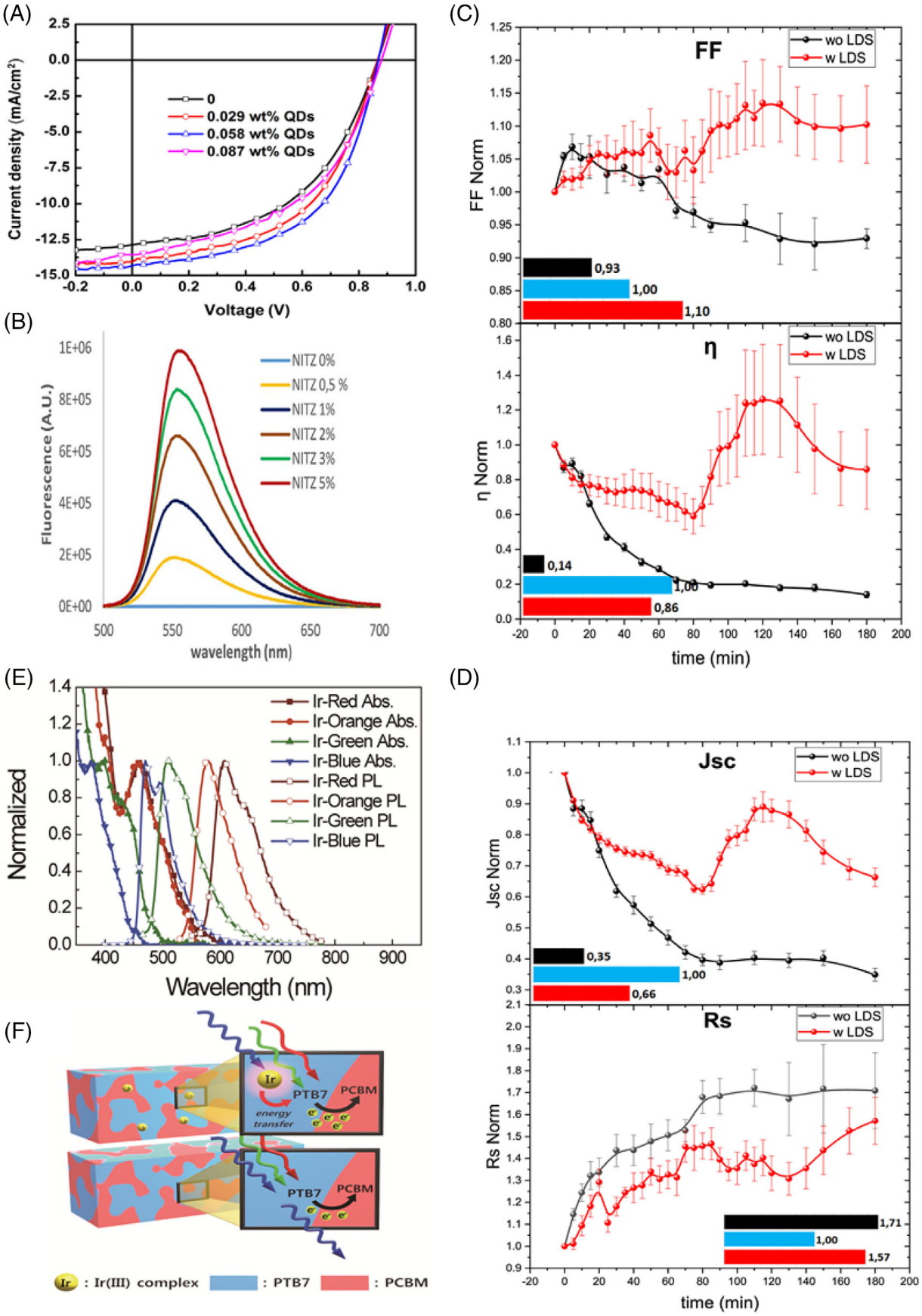


**FIGURE 10** (A) J-V characteristics of ITO/$TiO_2$/PCDTBT: PCBM: PFDTBT/$MoO_3$/Ag, devices at different doping concentration of PFDTBT quantum dots (QDs). Reproduced with permission.[119] Copyright © 2014, Elsevier B.V. (B) Emission spectra of NITZ solution at different concentrations. Reproduced with permission.[120] Copyright © 2017, Elsevier B.V. The normalized value of (C) FF and PCE, (D) $J_{sc}$ and series resistance (Rs), of CdS/ZnS based and control OSCs, as a function of light (AM 1.5) exposure time. Reproduced with permission.[121] copyright © 2021, Elsevier B.V. (E) Iridium-organic complexes absorption (solid symbols) and photoluminescence spectra (open symbols), (F) demonstration of iridium complex schematic energy transfer in the Ir (III) complexes doped PTB7: PC71BM active layer. Reproduced with permission.[122] Copyright © 2016, American Chemical Society

## 5 | SELECTION CRITERIA OF DC FOR OSCs

At present, a variety of organic donor/acceptor molecules have been investigated as photoactive layers and have shown different absorption behavior. In an OSCs, the donor's absorption region varies from 350 to 1050 nm wavelength and has different absorption peaks.[133–136] Moreover, recently developed NFAs have shown absorption towards near-infrared. The first criteria of selecting the DC system for solar cells is that their photoemission should be within the absorption region of the photoactive layer. And their absorption needs to be in the UV region and should not overlap with photoactive layer absorption. The PLQE of DC materials also needs to be high. In lanthanides and non-lanthanide nanophosphors, the emission property depends on the dopant element. The selection of the luminescent dopant can help in tuning the DC system's optical properties. For QDs luminescent materials, the optical properties can be tuned by regulating their sizes. The alignment of energy levels of different layers in OSCs has played a major role in improving overall photovoltaic performance. Moreover, the charge carrier (hole and electron) transport layers also play an essential role in energy level alignment as well as increasing or reducing the work function of electrodes.[137–139] To date, there are several metal salts, carbonate, fluoride, metal oxides, small molecules, polymers, and organometallic complexes reported as CTLs.[140] The deposition of the new layer above CTLs or doping into it might affect the energy level alignment between the photoactive layer and electrodes. Therefore, another essential selection criterion of the DC system; should form a favorable energy level alignment with charge carrier transport or photoactive layer. Chen et al. demonstrated the doping of Y, La, Ce, Nd, Sm, Gd, Tm, Yb, and Lu lanthanides into $TiO_2$ as an ETL and found that the Gd doping could form the better band alignment that helped in improving the $V_{oc}$ of the device.[141] The concentration of dopants also played a role in band alignment. Giordano et al. illustrated changes in the electronic properties of lithium (Li) doped $TiO_2$ films.[142] They revealed that the Li doping is responsible for 0.076 eV enhancement in $V_{oc}$ of the device after band alignment. The solvent selection for solution-processable DC is also the main requirement because the coating of the DC layer may harm the earlier deposited film, or it may get damaged by film coating on top of it. Additionally, the cost and processability of the DC system are also important factors to be consider and they should be compatible with the large area scale-up approach.

## 6 | CHALLENGES AND PROSPECTS FOR DC MATERIALS

The research on DC materials started a decade ago for OSCs. These were initially investigated for improving the performance of traditional inorganic solar cells. The performance improvement and material processing challenges for OSCs have subsequently risen and been noticed for further research. The impact of DC on solar cell performance is dependent on their absorption, photoemission, and PLQE values. There are various lanthanides, and non-lanthanides materials developed that improve the PCE and stability of solar cells. Nonetheless, the DC materials face a few challenges while implementing with OSCs and that need to be addressed before considering them for future solar cells applications. One of the main issues is the absorption width of DC materials.[143] The limited absorption-width issue can be improved by using the concept of attachment of sensitizer/ligand, and it can efficiently absorb the broad wavelength from 300–500 nm. Moreover, sensitizer/ligand effectively works as a light absorbent in the high-energy photon region and could transfer it to the nearby lanthanide whose enhanced emission strength. The selection of sensitizer/ligand materials is also a critical issue because they must work under continuous illumination and should have a high photo and thermal stability. Despite these issues, the overlapping of absorption and emission region of DC materials is also a new challenge that needs to be overcome. For this issue, QDs may be used as an alternative to solve the re-absorption losses as these have favorable broad absorption as well as tunable emission properties along with high quantum efficiency. QDs are also more appropriate to control the luminescence emission range as QDs size can be tuned to get the desired luminescence properties.[144,145] The high-temperature synthesis of lanthanide materials is also a bottleneck for future applications. As mentioned before, non-lanthanides DC has attracted attention for solar cell applications. Furthermore, the use of non-lanthanide materials might be promising as their processing requires low temperature, and they offer cost-effective solution-based coating.

## 7 | FUTURE PERSPECTIVES

A significant problem that bounds the efficiency of solar cells is their limitation to a full solar spectrum utilization. In the case of OSCs, there is a restriction to the absorption of donor and fullerene acceptor molecules even after tuning the bandgap, particularly in the infra-red and high-energy photon region. Recently, the NFAs have been synthesized, having a low bandgap and high absorption coefficient, which has replaced the fullerene derivatives as acceptors.[146] The NFAs show adequate absorption towards the near-infrared region. However, they are still inadequate to cover a large incident solar spectrum. Recently, it has been found that the DC strategy could overcome this problem and improve the coverage of incident light solar spectrum towards high energy photons, and this would increase the efficiency of the devices in the near future. Moreover, the photo-induced degradation of OSCs is still a major concern that can be overcome by DC strategy. From the device point of view, most of the DC coatings have been applied on the front side of the transparent electrode, and it might be difficult to maintain an extra layer. Also, on the front side of the device, an extra deposition of layer required an environmental protection. To be specific, the DC materials require a dual functional property, and it could be achieved, for example, by doping the lanthanide or non-lanthanide material into the charge transport layer materials which may work as the charge carriers transport layer as well as DC layer. The doping of DC materials in the photoactive layer also has been proposed. The maximum utilization of solar spectrum from NIR to UV for generating the high PCE of solar cells is the priority. The development of a single layer by incorporating the DC and up-conversion (UC) materials would-be a cost-effective method for modifying

the incident solar spectram. Implementing the DC and UC mechanisms together could be the key. The proof of concept has been introduced by Yao et al.[147] in which $Er^{3+}$ and $Yb^{3+}$, and $Eu^{3+}$ and $Tb^{3+}$ were doped in ZnO as UC and DC materials, respectively, for the DSSC device. By combining these two materials, the 70% performance enhancement has been reported as compared to the control device. Both layers have improved the $J_{sc}$ (6.38 to 10.13 mA/cm$^2$), as well as the $V_{oc}$ (0.70–0.76 V). Li et al. also incorporated the $Yb^{3+}$, $Er^{3+}$/$Tm^{3+}$ as a UC and $NaYF_4$ and $Eu(TTA)_2(Phen)$ MAA as a DC in PSCs, and the device PCE was improved by 19.7% (from 16% to 19.5%).[148] There are a few DC and UC compound have been reported, and showed relatively high energy transfer efficiency and could be applied for OSCs.[149–151] Similarly, materials having absorption in both UV and IR regions, with the corresponding emission in the visible range, could be synthesized and explored. From the application point of view, there are various areas where DC-based devices can perform outstandingly. For example, in space, where plenty of UV radiation is available and could be utilized efficiently for solar cells. In 2002, Bailey from NASA reported that the OSCs are more promising for space applications.[152–155] The researchers are taking an interest in investigating the OSCs for space applications, as space is free of oxygen and moisture.[156–158] Besides it, space is free of ozone and moisture, and these do not block the UV photons. The incorporation of DC would be vastly beneficial for energy conversion and photostability perspective.

## 8 | SUMMARY

The DC materials for OSCs is an emerging field in photovoltaics, which has been discussed in this review. In summary, we have reviewed the lanthanides and non-lanthanides DC materials, their spectral conversion properties, operating phenomenon, along with working progress in the OSCs. The role of the lanthanides and non-lanthanide doped complex materials layer as spectral modifier or converters and their benefit in improving performance parameters as well as the stabilities of OSCs is demonstrated. In DC materials, the $Eu^{3+}$ incorporated OSCs devices are widely reported and have shown an impact on efficiency and stability improvement. Yttrium, Cerium, and Terbium-based DC compounds are also being implemented for OSCs, and their performance, as well as stability improvement, are not so impressive. Besides, their deposition required high temperature and high vacuum sophisticated system, whereas the $Eu^{3+,}$ as well as $Sm^{3+}$ based compounds, are solution-processable, which is the first requirement from a cost-effective point of view. In non-lanthanides, ZnO doped with Na, and the incorporation of ZnO nanoparticles in the PMMA polymer, has been a good choice as DC and has shown better stability in OSCs. Furthermore, these doped materials can be utilized as a dual function layer. The QDs are also encouraged as DC materials. These have fine energy bandgap tuning properties, which make them attractive, as well as the overlapping of absorption and emission spectra, can be prevented. Finally, this review might be of great interest for researchers with both physics and chemistry backgrounds to develop various durable, cost-effective, and enhanced efficiency materials for DC-based OSCs. Most of the materials reported for incident light spectrum modification have quantum efficiency less than unity and have less impact on device performance. It could be worth investigating materials having quantum efficiency higher than unity for future OSCs applications. The doping of DC in the charge transport layer or a coating on top of it could be worth investigating for future application, as it could improve the film's morphology and energy band alignment.

## ACKNOWLEDGMENTS

The author Ram Datt acknowledges the SPECIFIC Innovation and Knowledge Centre (EP/N020863/1) for funding. Author Swati Bishnoi sincerely acknowledges the Council of Scientific & Industrial Research (CSIR) for providing a Research Associate fellowship (#31/1(0494)/2018-EMR-1).

## CONFLICT OF INTEREST

The authors declare that they have no conflict to declare.

## DATA AVAILABILITY STATEMENT

None.

## ORCID

*Wing Chung Tsoi* https://orcid.org/0000-0003-3836-5139

## REFERENCES

1. N. S. Lewis, D. G. Nocera, *Proc. Natl. Acad. Sci*. **2006**, *103*, 15729.
2. K. A. Mazzio, C. K. Luscombe, *Chem. Soc. Rev.* **2015**, *44*, 78.
3. M. Riede, D. Spoltore, K. Leo, *Adv. Energy Mater.* **2021**, *11*, 2002653.
4. K. Fukuda, K. Yu, T. Someya, *Adv. Energy Mater.* **2020**, *10*, 2000765.
5. Q. Liu, Y. Jiang, K. Jin, J. Qin, J. Xu, W. Li, J. Xiong, J. Liu, Z. Xiao, K. Sun, S. Yang, X. Zhang, L. Ding, *Sci. Bull.* **2020**, *65*, 272.
6. M. B. Salim, R. Nekovei, R. Jeyakumar, *Sol. Energy* **2020**, *198*, 160.
7. J. Wang, Z. Zheng, Y. Zu, Y. Wang, X. Liu, S. Zhang, M. Zhang, J. Hou, *Adv. Mater.* **2021**, *2102787*, 1.
8. R. Datt, S. Arya, S. Bishnoi, R. Gupta, V. Gupta, A. Khosla, *Microsyst. Technol.* **2019**, *28*, 269. https://link.springer.com/article/10.1007/s00542-019-04687-7.
9. B. Arredondo, B. Romero, M. J. Beliatis, G. del Pozo, D. Martín-Martín, J. C. Blakesley, G. Dibb, F. C. Krebs, S. A. Gevorgyan, F. A. Castro, *Sol. Energy Mater. Sol. Cells* **2018**, *176*, 397.
10. P. Cheng, X. Zhan, *Chem. Soc. Rev.* **2016**, *45*, 2544.
11. I. A. Channa, A. Distler, M. Zaiser, C. J. Brabec, H. Egelhaaf, *Adv. Energy Mater.* **2019**, *9*, 1900598.
12. Q. Lu, Z. Yang, X. Meng, Y. Yue, M. A. Ahmad, W. Zhang, S. Zhang, Y. Zhang, Z. Liu, W. Chen, *Adv. Funct. Mater.* **2021**, *31*, 2100151.
13. S. K. Gaddam, R. Pothu, R. Boddula, *J. Mater*. **2021**, *7*, 920.
14. M. Giannouli, V. M. Drakonakis, A. Savva, P. Eleftheriou, G. Florides, S. A. Choulis, *ChemPhysChem* **2015**, *16*, 1134.
15. A. Classen, T. Heumueller, I. Wabra, J. Gerner, Y. He, L. Einsiedler, N. Li, G. J. Matt, A. Osvet, X. Du, A. Hirsch, C. J. Brabec, *Adv. Energy Mater.* **2019**, *9*, 1902124.
16. J. B. Patel, P. Tiwana, N. Seidler, G. E. Morse, O. R. Lozman, M. B. Johnston, L. M. Herz, *ACS Appl. Mater. Interfaces* **2019**, *11*, 21543.
17. B. Liu, Y. Han, Z. Li, H. Gu, L. Yan, Y. Lin, Q. Luo, S. Yang, C.-Q. Ma, *Sol. RRL* **2021**, *5*, 2000638.
18. N. Y. Doumon, G. Wang, X. Qiu, A. J. Minnaard, R. C. Chiechi, L. J. A. Koster, *Sci. Rep.* **2019**, *9*, 4350.
19. Y. Jiang, L. Sun, F. Jiang, C. Xie, L. Hu, X. Dong, F. Qin, T. Liu, L. Hu, X. Jiang, Y. Zhou, *Mater. Horizons* **2019**, *6*, 1438.
20. S. Park, H. J. Son, *J. Mater. Chem. A* **2019**, *7*, 25830.
21. S. Rasool, V. Van Doan, H. K. Lee, S. K. Lee, J.-C. Lee, S.-J. Moon, W. W. So, C. E. Song, W. S. Shin, *Thin Solid Films* **2019**, *669*, 42.
22. S. B. Sapkota, M. Fischer, B. Zimmermann, U. Würfel, *Sol. Energy Mater. Sol. Cells* **2014**, *121*, 43.
23. A. B. Belay, W. Zhou, R. Krueger, K. O. Davis, Ü. Alver, N. Sorloaica-Hickman, *IEEE J. Photovoltaics* **2012**, *2*, 148.
24. Q. Liu, J. Toudert, F. Liu, P. Mantilla-Perez, M. M. Bajo, T. P. Russell, J. Martorell, *Adv. Energy Mater.* **2017**, *7*, 1701201.
25. T. Liu, Y. Zhang, Y. Shao, R. Ma, Z. Luo, Y. Xiao, T. Yang, X. Lu, Z. Yuan, H. Yan, Y. Chen, Y. Li, *Adv. Funct. Mater.* **2020**, *30*, 2000456.

26. Y. Lin, Y. Firdaus, M. I. Nugraha, F. Liu, S. Karuthedath, A. H. Emwas, W. Zhang, A. Seitkhan, M. Neophytou, H. Faber, E. Yengel, I. McCulloch, L. Tsetseris, F. Laquai, T. D. Anthopoulos, *Adv. Sci.* **2020**, *7*, 1.
27. E. M. Speller, A. J. Clarke, J. Luke, H. K. H. Lee, J. R. Durrant, N. Li, T. Wang, H. C. Wong, J.-S. Kim, W. C. Tsoi, Z. Li, *J. Mater. Chem. A* **2019**, *7*, 23361.
28. W. Chen, Q. Zhang, *J. Mater. Chem. C* **2017**, *5*, 1275.
29. W. Chen, X. Yang, G. Long, X. Wan, Y. Chen, Q. Zhang, *J. Mater. Chem. C* **2015**, *3*, 4698.
30. H. Sun, X. Song, J. Xie, P. Sun, P. Gu, C. Liu, F. Chen, Q. Zhang, Z.-K. Chen, W. Huang, *ACS Appl. Mater. Interfaces* **2017**, *9*, 29924.
31. A. Azeez, K. S. Narayan, *J. Phys. Chem. C* **2021**, *125*, 12531.
32. A. J. Clarke, J. Luke, R. Meitzner, J. Wu, Y. Wang, H. K. H. Lee, E. M. Speller, H. Bristow, H. Cha, M. J. Newman, K. Hooper, A. Evans, F. Gao, H. Hoppe, I. McCulloch, U. S. Schubert, T. M. Watson, J. R. Durrant, W. C. Tsoi, J.-S. Kim, Z. Li, *Cell Rep. Phys. Sci.* **2021**, *2*, 100498.
33. J. Jeong, J. Seo, S. Nam, H. Han, H. Kim, T. D. Anthopoulos, D. D. C. Bradley, Y. Kim, *Adv. Sci.* **2016**, *3*, 1500269.
34. W. Shockley, H. J. Queisser, *J. Appl. Phys.* **1961**, *32*, 510.
35. X. Ma, A. Zeng, J. Gao, Z. Hu, C. Xu, J. H. Son, S. Y. Jeong, C. Zhang, M. Li, K. Wang, H. Yan, Z. Ma, Y. Wang, H. Y. Woo, F. Zhang, *Natl. Sci. Rev.* **2021**, *8*, 527.
36. X. Wang, Q. Sun, J. Gao, J. Wang, C. Xu, X. Ma, F. Zhang, *Energies* **2021**, *14*, 4200.
37. W. Xu, X. Ma, J. H. Son, S. Y. Jeong, L. Niu, C. Xu, S. Zhang, Z. Zhou, J. Gao, H. Y. Woo, J. Zhang, J. Wang, F. Zhang, *Small* **2021**, *2104215*, 2104215.
38. R. Datt, R. Sharma, S. Bishnoi, V. Gupta, *Mater. Lett.* **2019**, *251*, 122.
39. J. Gao, W. Gao, X. Ma, Z. Hu, C. Xu, X. Wang, Q. An, C. Yang, X. Zhang, F. Zhang, *Energy Environ. Sci.* **2020**, *13*, 958.
40. J. Gao, J. Wang, Q. An, X. Ma, Z. Hu, C. Xu, X. Zhang, F. Zhang, *Sci. China Chem.* **2020**, *63*, 83.
41. B. SambathKumar, P. Shyam Vinod Kumar, F. S. Deepakrao, S. S. Kumar Iyer, V. Subramanian, R. Datt, V. Gupta, S. Chand, N. Somanathan, *J. Phys. Chem. C* **2016**, *120*, 26609.
42. T. Zhu, L. Zheng, Z. Xiao, X. Meng, L. Liu, L. Ding, X. Gong, *Sol. RRL* **2019**, *3*, 1900322.
43. P. J. Jadhav, A. Mohanty, J. Sussman, J. Lee, M. A. Baldo, *Nano Lett.* **2011**, *11*, 1495.
44. T. C. Wu, N. J. Thompson, D. N. Congreve, E. Hontz, S. R. Yost, T. Van Voorhis, M. A. Baldo, *Appl. Phys. Lett.* **2014**, *104*, 193901.
45. K. Aryanpour, J. A. Muñoz, S. Mazumdar, *J. Phys. Chem. C* **2013**, *117*, 4971.
46. D. N. Congreve, J. Lee, N. J. Thompson, E. Hontz, S. R. Yost, P. D. Reusswig, M. E. Bahlke, S. Reineke, T. Van Voorhis, M. A. Baldo, *Science (80-.).* **2013**, *340*, 334.
47. G. Lanzani, S. Stagira, G. Cerullo, S. De Silvestri, D. Comoretto, I. Moggio, C. Cuniberti, G. Musso, G. Dellepiane, *Chem. Phys. Lett.* **1999**, *313*, 525.
48. C. C. Gradinaru, J. T. M. Kennis, E. Papagiannakis, I. H. M. van Stokkum, R. J. Cogdell, G. R. Fleming, R. A. Niederman, R. van Grondelle, *Proc. Natl. Acad. Sci.* **2001**, *98*, 2364.
49. C. Jundt, G. Klein, B. Sipp, J. Le Moigne, M. Joucla, A. A. Villaeys, *Chem. Phys. Lett.* **1995**, *241*, 84.
50. R. E. Merrifield, P. Avakian, R. P. Groff, *Chem. Phys. Lett.* **1969**, *3*, 155.
51. G. Klein, R. Voltz, M. Schott, *Chem. Phys. Lett.* **1972**, *16*, 340.
52. P. J. Budden, L. R. Weiss, M. Müller, N. A. Panjwani, S. Dowland, J. R. Allardice, M. Ganschow, J. Freudenberg, J. Behrends, U. H. F. Bunz, R. H. Friend, *Nat. Commun.* **2021**, *12*, 1527.
53. T. Trupke, M. A. Green, P. Würfel, *J. Appl. Phys.* **2002**, *92*, 1668. https://aip.scitation.org/doi/abs/10.1063/1.1492021.
54. J. de Wild, A. Meijerink, J. K. Rath, W. G. J. H. M. van Sark, R. E. I. Schropp, *Energy Environ. Sci.* **2011**, *4*, 4835.
55. T. Ameri, P. Khoram, J. Min, C. J. Brabec, *Adv. Mater.* **2013**, *25*, 4245.
56. W. Li, Q. Song, X. Sun, M. Wang, H. Wu, X. Ding, X. Hou, *Sci. China Phys. Mech. Astron.* **2010**, *53*, 288.
57. D. Di Carlo Rasi, R. A. J. Janssen, *Adv. Mater.* **2019**, *31*, 1806499.
58. H. Fu, Z. Wang, Y. Sun, *Sol. RRL* **2018**, *2*, 1700158.
59. B. S. Richards, *Sol. Energy Mater. Sol. Cells* **2006**, *90*, 2329.
60. Z. Hosseini, N. Taghavinia, E. Wei-Guang Diau, *ChemPhysChem* **2017**, *18*, 3292.
61. X. Huang, S. Han, W. Huang, X. Liu, *Chem. Soc. Rev.* **2013**, *42*, 173.
62. B. Ehrler, N. Yanai, L. Nienhaus, *J. Chem. Phys.* **2021**, *154*, 070401. https://aip.scitation.org/doi/full/10.1063/5.0045323.
63. R. R. Tykwinski, D. M. Guldi, *ChemPhotoChem* **2021**, *5*, 392.
64. J. -Y. Chen, Y. -C. Chiu, C. -C. Shih, W. -C. Wu, W. -C. Chen, *J. Mater. Chem. A* **2015**, *3*, 15039.
65. Q. Y. Zhang, X. Y. Huang, *Prog. Mater. Sci.* **2010**, *55*, 353.
66. J. T. van Wijngaarden, S. Scheidelaar, T. J. H. Vlugt, M. F. Reid, A. Meijerink, *Phys. Rev. B* **2010**, *81*, 155112.
67. R. T. Wegh, H. Donker, K. D. Oskam, A. Meijerink, *Science (80-.).* **1999**, *283*, 663.
68. J. McKittrick, L. E. Shea-Rohwer, *J. Am. Ceram. Soc.* **2014**, *97*, 1327.
69. J. S. Steckel, J. Ho, C. Hamilton, J. Xi, C. Breen, W. Liu, P. Allen, S. Coe-Sullivan, *J. Soc. Inf. Disp.* **2015**, *23*, 294.
70. T. Forster, *Naturwissenschaften* **1946**, *33*, 166.
71. D. L. Dexter, *J. Chem. Phys.* **1953**, *21*, 836.
72. Z. Hosseini, T. Ghanbari, *RSC Adv.* **2018**, *8*, 31502.
73. J. S. Avery, *Proc. Phys. Soc.* **1966**, *88*, 559. https://iopscience.iop.org/article/10.1088/0370-1328/88/1/302.
74. D. L. Andrews, *Chem. Phys.* **1989**, *135*, 195.
75. H. Kuhn, *J. Chem. Phys.* **1970**, *53*, 101.
76. K. Oskam, R. Wegh, H. Donker, E. V. van Loef, A. Meijerink, *J. Alloys Compd.* **2000**, *300–301*, 421.
77. P. Vergeer, T. J. H. Vlugt, M. H. F. Kox, M. I. den Hertog, J. P. J. M. van der Eerden, A. Meijerink, *Phys. Rev. B* **2005**, *71*, 014119.
78. D.-C. Yu, R. Martín-Rodríguez, Q.-Y. Zhang, A. Meijerink, F. T. Rabouw, *Light Sci. Appl.* **2015**, *4*, e344.
79. M. J. Y. Tayebjee, D. R. McCamey, T. W. Schmidt, *J. Phys. Chem. Lett.* **2015**, *6*, 2367.
80. J. Kalowekamo, E. Baker, *Sol. Energy* **2009**, *83*, 1224.
81. J. Guo, J. Min, *Adv. Energy Mater.* **2019**, *9*, 1802521.
82. A. Gambhir, P. Sandwell, J. Nelson, *Sol. Energy Mater. Sol. Cells* **2016**, *156*, 49.
83. A. Le Donne, M. Acciarri, D. Narducci, S. Marchionna, S. Binetti, *Prog. Photovolt. Res. Appl.* **2009**, *17*, 519.
84. H. -J. Kim, J. -S. Song, D. -Y. Lee, W. -J. Lee, *Trans. Electr. Electron. Mater.* **2004**, *5*, 89.
85. J. Liu, Q. Yao, Y. Li, *Appl. Phys. Lett.* **2006**, *88*, 173119.
86. B. S. Richards, *Sol. Energy Mater. Sol. Cells* **2006**, *90*, 1189.
87. C. Strümpel, M. McCann, G. Beaucarne, V. Arkhipov, A. Slaoui, V. Švrček, C. del Cañizo, I. Tobias, *Sol. Energy Mater. Sol. Cells* **2007**, *91*, 238.
88. W. Bin Hung, J. Y. Chen, K. W. Sung, T. M. Chen, *Ceram. Process. Res.* **2014**, *15*, 157.
89. L. Dumont, J. Cardin, P. Benzo, M. Carrada, C. Labbé, A. L. Richard, D. C. Ingram, W. M. Jadwisienczak, F. Gourbilleau, *Sol. Energy Mater. Sol. Cells* **2016**, *145*, 84.
90. I. Vivaldo, J. Carrillo, O. López, S. Jiménez, J. Martínez, D. Murias, J. A. López, *Int. J. Energy Res.* **2017**, *41*, 410.
91. H. Yao, Q. Tang, *Sol. Energy* **2020**, *211*, 446.
92. H. -C. Chen, C. -C. Lin, H. -V. Han, K. -J. Chen, Y. -L. Tsai, Y. -A. Chang, M. -H. Shih, H. -C. Kuo, P. Yu, *Sol. Energy Mater. Sol. Cells* **2012**, *104*, 92.
93. C. -C. Lin, H. -C. Chen, Y. L. Tsai, H. -V. Han, H. -S. Shih, Y. -A. Chang, H. -C. Kuo, P. Yu, *Opt. Express* **2012**, *20*, A319.
94. W. -J. Ho, J. -J. Liu, Z. -X. Lin, H. -P. Shiao, *Nanomater.* **2019**, *9*, 1518.
95. D. Gao, H. Zheng, X. Zhang, Z. Fu, Z. Zhang, Y. Tian, M. Cui, *Appl. Phys. Lett.* **2011**, *98*, 011907.
96. W. Xu, H. Song, D. Yan, H. Zhu, Y. Wang, S. Xu, X. Bai, B. Dong, Y. Liu, *J. Mater. Chem.* **2011**, *21*, 12331.
97. O. Örnek, Z. A. Kösemen, S. Öztürk, B. Canımkurbey, Ş. Fındık, M. Erkovan, A. Kösemen, *Surf. Interfaces* **2017**, *9*, 64.
98. J. Jiao, S. Gai, Y. Li, W. Shen, J. Tang, Y. Wang, L. Huang, J. Liu, W. Wang, L. A. Belfiore, *Electrochim. Acta* **2018**, *260*, 959.
99. R. Datt, S. Bishnoi, R. Gupta, D. Haranath, S. N. Sharma, G. Gupta, S. Arya, S. Kumar, V. Gupta, *Synth. Met.* **2019**, *255*, 116112.
100. F. Bu, W. Shen, X. Zhang, Y. Wang, L. A. Belfiore, J. Tang, *Nanomaterials* **2020**, *10*, 80.
101. T. Mohammad, V. Bharti, V. Kumar, S. Mudgal, V. Dutta, *Org. Electron.* **2019**, *66*, 242.
102. M. Dusza, M. Stefanski, M. Wozniak, D. Hreniak, Y. Gerasymchuk, L. Marciniak, F. Granek, W. Strek, *J. Lumin.* **2016**, *169*, 857.

103. F. Otieno, M. Airo, R. M. Erasmus, D. G. Billing, A. Quandt, D. Wamwangi, *RSC Adv.* **2018**, *8*, 29274.
104. S. Bishnoi, V. Gupta, C. Sharma, D. Haranath, S. Naqvi, M. Kumar, G. D. Sharma, S. Chand, *Appl. Phys. Lett.* **2016**, *109*, 023902.
105. Q. Li, Y. Yuan, T. Wei, Y. Li, Z. Chen, X. Jin, Y. Qin, W. Sun, *Sol. Energy Mater. Sol. Cells* **2014**, *130*, 426.
106. Q. Li, Y. Yuan, Z. Chen, X. Jin, T. Wei, Y. Li, Y. Qin, W. Sun, *ACS Appl. Mater. Interfaces* **2014**, *6*, 12798.
107. Z. Chen, Q. Li, C. Chen, J. Du, J. Tong, X. Jin, Y. Li, Y. Yuan, Y. Qin, T. Wei, W. Sun, *Phys. Chem. Chem. Phys.* **2014**, *16*, 24499.
108. K. Binnemans, P. T. Jones, T. Müller, L. Yurramendi, *J. Sustain. Metall.* **2018**, *4*, 126.
109. C. N. R. Rao, G. V. Subba Rao, *Phys. Status Solidi* **1970**, *1*, 597.
110. S. Laurent, S. Boutry, R. N. Muller, *Iron Oxide Nanoparticles for Biomedical Applications*, Elsevier Amsterdam, NL **2018**.
111. R. Datt, Suman, A. Bagui, A. Siddiqui, R. Sharma, V. Gupta, S. Yoo, S. Kumar, S. P. Singh, *Sci. Rep.* **2019**, *9*, 8529.
112. H. Sun, J. Weickert, H. C. Hesse, L. Schmidt-Mende, *Sol. Energy Mater. Sol. Cells* **2011**, *95*, 3450.
113. S. Bishnoi, V. Gupta, C. Sharma, D. Haranath, M. Kumar, S. Chand, *Org. Electron.* **2016**, *38*, 193.
114. Y.-T. Cho, H. Su, I.-C. Huang, C.-Y. Lai, Y.-D. Tsai, *Anal. Methods* **2019**, *11*, 6013.
115. S. M. A. Karim, R. Nomura, T. Masuda, *J. Polym. Sci. Part A Polym. Chem.* **2001**, *39*, 3130.
116. W.-E. Lee, H. Park, G. Kwak, *Chem. Commun.* **2011**, *47*, 659.
117. D. C. Han, G. Kwak, Y. B. Kim, J. J. Bae, W. H. Lee, Y.-S. Seo, J. H. Byun, S. W. Kang, *J. Nanosci. Nanotechnol.* **2014**, *14*, 5937.
118. M. Prosa, A. Sagnella, T. Posati, M. Tessarolo, M. Bolognesi, S. Cavallini, S. Toffanin, V. Benfenati, M. Seri, G. Ruani, M. Muccini, R. Zamboni, *RSC Adv.* **2014**, *4*, 44815.
119. C. Liu, W. Guo, H. Jiang, L. Shen, S. Ruan, D. Yan, *Org. Electron.* **2014**, *15*, 2632.
120. O. Ourahmoun, T. Trigaud, B. Ratier, M. S. Belkaid, L. Galmiche, P. Audebert, *Synth. Met.* **2017**, *234*, 106.
121. R. M. Aoki, E. T. dos S Torres, J. P. A. de Jesus, S. A. Lourenço, R. V. Fernandes, E. Laureto, M. A. Toledo da Silva, *J. Lumin.* **2021**, *237*, 118178.
122. H.-T. Kim, J. H. Seo, J. H. Ahn, M.-J. Baek, H.-D. Um, S. Lee, D.-H. Roh, J.-H. Yum, T. J. Shin, K. Seo, T.-H. Kwon, *ACS Energy Lett.* **2016**, *1*, 991.
123. D. Svechkarev, A. M. Mohs, *Curr. Med. Chem.* **2019**, *26*, 4042.
124. D. Joly, L. Pellejà, S. Narbey, F. Oswald, J. Chiron, J. N. Clifford, E. Palomares, R. Demadrille, *Sci. Rep.* **2015**, *4*, 4033.
125. J.-Y. Chen, C. K. Huang, W. B. Hung, K. W. Sun, T. M. Chen, *Sol. Energy Mater. Sol. Cells* **2014**, *120*, 168.
126. R. V. Fernandes, A. Urbano, J. L. Duarte, N. Bristow, J. Kettle, E. Laureto, *J. Lumin.* **2018**, *203*, 165.
127. A. Pardo Perdomo, R. Vignoto Fernandes, N. J. Artico Cordeiro, F. Franchello, M. A. Toledo da Silva, J. Leonil Duarte, E. Laureto, *J. Appl. Phys.* **2020**, *128*, 035502.
128. H. C. Lim, J.-J. Koo, J. Il Kim, J.-K. Lee, Z. H. Kim, J.-I. Hong, *New J. Chem.* **2019**, *43*, 18843.
129. K. E. Jasim, *Solar Cells - New Approaches and Reviews*; InTechOpen, London **2015**.
130. E. H. M. Sakho, O. S. Oluwafemi, *Nanomaterials for Solar Cell Applications*; Elsevier Inc., Amsterdam, NL **2019**.
131. H. Xu, R. Chen, Q. Sun, W. Lai, Q. Su, W. Huang, X. Liu, *Chem. Soc. Rev.* **2014**, *43*, 3259.
132. T. R. Cook, Y. R. Zheng, P. J. Stang, *Chem. Rev.* **2013**, *113*, 734.
133. K. Rahimi, I. Botiz, J. O. Agumba, S. Motamen, N. Stingelin, G. Reiter, *RSC Adv.* **2014**, *4*, 11121.
134. V. Gupta, V. Bharti, M. Kumar, S. Chand, A. J. Heeger, *Adv. Mater.* **2015**, *27*, 4398.
135. W. Zhao, D. Qian, S. Zhang, S. Li, O. Inganäs, F. Gao, J. Hou, *Adv. Mater.* **2016**, *28*, 4734.
136. Y. Liu, J. Zhao, Z. Li, C. Mu, W. Ma, H. Hu, K. Jiang, H. Lin, H. Ade, H. Yan, *Nat. Commun.* **2014**, *5*, 5293.
137. T. Oida, K. Harafuji, *Jpn. J. Appl. Phys.* **2012**, *51*, 091601.
138. S. Shao, M. A. Loi, *Adv. Mater. Interfaces* **2020**, *7*, 1901469.
139. M. Deng, W. Shi, C. Zhao, B. Chen, Y. Shen, *Front. Optoelectron.* **2015**, *8*, 269.
140. D. Ouyang, Z. Huang, W. C. H. Choy, *Adv. Funct. Mater.* **2019**, *29*, 1804660.
141. C. Chen, D. Liu, Y. Wu, W. Bi, X. Sun, X. Chen, W. Liu, L. Xu, H. Song, Q. Dai, *Nano Energy* **2018**, *53*, 849.
142. F. Giordano, A. Abate, J. P. Correa Baena, M. Saliba, T. Matsui, S. H. Im, S. M. Zakeeruddin, M. K. Nazeeruddin, A. Hagfeldt, M. Graetzel, *Nat. Commun.* **2016**, *7*, 10379.
143. W. G. J. H. M. van, A. Meijerink, R. E. I. Schropp, *Third Generation Photovoltaics*, InTechOpen, London **2012**.
144. U. T. D. Thuy, L. A. Tu, N. T. Loan, T. T. K. Chi, N. Q. Liem, *Opt. Mater.* **2016**, *53*, 34.
145. S. Kim, B. Fisher, H.-J. Eisler, M. Bawendi, *J. Am. Chem. Soc.* **2003**, *125*, 11466.
146. A. Wadsworth, M. Moser, A. Marks, M. S. Little, N. Gasparini, C. J. Brabec, D. Baran, I. McCulloch, *Chem. Soc. Rev.* **2019**, *48*, 1596.
147. N. Yao, J. Huang, K. Fu, X. Deng, M. Ding, M. Shao, X. Xu, *Electrochim. Acta* **2015**, *154*, 273.
148. H. Li, C. Chen, J. Jin, W. Bi, B. Zhang, X. Chen, L. Xu, D. Liu, Q. Dai, H. Song, *Nano Energy* **2018**, *50*, 699.
149. P. A. Loiko, N. M. Khaidukov, J. Méndez-Ramos, E. V. Vilejshikova, N. A. Skoptsov, K. V. Yumashev, *J. Lumin.* **2016**, *170*, 1.
150. A. Bahadur, R. S. Yadav, R. V. Yadav, S. B. Rai, *J. Solid State Chem.* **2017**, *246*, 81.
151. K. -T. Lee, J. -H. Park, S. J. Kwon, H. -K. Kwon, J. Kyhm, K. -W. Kwak, H. S. Jang, S. Y. Kim, J. S. Han, S. -H. Lee, D. -H. Shin, H. Ko, I. -K. Han, B. -K. Ju, S. -H. Kwon, D. -H. Ko, *Nano Lett.* **2015**, *15*, 2491.
152. S. G. Bailey, J. D. Harris, A. F. Hepp, E. J. Anglin, R. P. Raffaelle, H. R. Clark, S. T. P. Gardner & S. S. Sun IECEC '02. 2002 37th Intersociety Energy Conversion Engineering Conference, 2002, pp. 191-196
153. H. K. H. Lee, J. R. Durrant, Z. Li, W. C. Tsoi, *J. Mater. Res.* **2018**, *33*, 1902.
154. J. Barbé, A. Pockett, V. Stoichkov, D. Hughes, H. K. H. Lee, M. Carnie, T. Watson, W. C. Tsoi, *J. Mater. Chem. C* **2020**, *8*, 1715.
155. J. Barbé, H. K. H. Lee, H. Toyota, K. Hirose, S. Sato, T. Ohshima, K. C. Heasman, W. C. Tsoi, *Appl. Phys. Lett.* **2018**, *113*, 183301.
156. I. Cardinaletti, T. Vangerven, S. Nagels, R. Cornelissen, D. Schreurs, J. Hruby, J. Vodnik, D. Devisscher, J. Kesters, J. D'Haen, A. Franquet, V. Spampinato, T. Conard, W. Maes, W. Deferme, J. V. Manca, *Sol. Energy Mater. Sol. Cells* **2018**, *182*, 121.
157. J.-S. Huang, M. D. Kelzenberg, P. Espinet-Gonzalez, C. Mann, D. Walker, A. Naqavi, N. Vaidya, E. Warmann, H. A. Atwater, *2017 IEEE 44th Photovolt. Spec. Conf.*, IEEE, Washington, DC **2017**, 1248.
158. O. Malinkiewicz, M. Imaizumi, S. B. Sapkota, T. Ohshima, S. Öz, *Emerg. Mater.* **2020**, *3*, 9.


## AUTHOR BIOGRAPHIES

**Ram Datt** is working as Research Staff in the SPECIFIC, Faculty of Science and Engineering, Swansea University, Swansea, United Kingdom. He has completed his Ph.D. (2019) in Engineering Science from CSIR- National Physical Laboratory, New Delhi, India, in the field of organic solar cells. Currently, he is working on organic and perovskite solar cells for indoor and space applications and down-conversion materials for photovoltaic applications.

**Swati Bishnoi** is working as a Research Associate in CSIR-National Physical Laboratory (NPL), New Delhi, India. She has completed a Ph.D. in Engineering Science from CSIR-NPL, New Delhi in 2018. She is working in the area of luminescent nanomaterials, down-conversion, up-conversion phosphors, and quantum

dots for achieving spectral conversion for photovoltaic applications.

**Wing Chung Tsoi** is an Associate Professor at the Faculty of Science and Engineering, Swansea University, Swansea, United Kingdom. He obtained his Ph.D. from the University of Hull. His research interests include organic and perovskite photovoltaic cells for indoor and aerospace applications, organic semi-transparent solar cells, their stability, and advanced characterization techniques to study opto-electronic devices. Dr. Tsoi has published 74 papers, given 33 invited talks, and was awarded the 2021 Royal Microscopy Society Medal for Innovation in Applied Microscopy for Engineering and Physical Sciences.

**How to cite this article:** R. Datt, S. Bishnoi, H. K. H. Lee, S. Arya, S. Gupta, V. Gupta, W. C. Tsoi. *Aggregate* **2022**, e185.
https://doi.org/10.1002/agt2.185